



# Refined explicit integration of elastoplastic models with automatic error control

Elastoplastic  
models

121

Scott W. Sloan, Andrew J. Abbo and Daichao Sheng  
*Department of Civil, Surveying and Environmental Engineering,  
University of Newcastle, New South Wales, Australia*

**Keywords** *Integration, Stress analysis, Algorithms, Elastoplasticity*

**Abstract** *Effective explicit algorithms for integrating complex elastoplastic constitutive models, such as those belonging to the Cam clay family, are described. These automatically divide the applied strain increment into subincrements using an estimate of the local error and attempt to control the global integration error in the stresses. For a given scheme, the number of substeps used is a function of the error tolerance specified, the magnitude of the imposed strain increment, and the non-linearity of the constitutive relations. The algorithms build on the work of Sloan in 1987 but include a number of important enhancements. The steps required to implement the integration schemes are described in detail and results are presented for a rigid footing resting on a layer of Tresca, Mohr-Coulomb, modified Cam clay and generalised Cam clay soil. Explicit methods with automatic substepping and error control are shown to be reliable and efficient for these models. Moreover, for a given load path, they are able to control the global integration error in the stresses to lie near a specified tolerance. The methods described can be used for exceedingly complex constitutive laws, including those with a non-linear elastic response inside the yield surface. This is because most of the code required to program them is independent of the precise form of the stress-strain relations. In contrast, most of the implicit methods, such as the backward Euler return scheme, are difficult to implement for all but the simplest soil models.*

## 1. Introduction

A key step in non-linear finite element analysis involves integrating the constitutive relations to obtain the unknown increment in the stresses. These relations define a set of ordinary differential equations and methods for integrating them are usually classified as explicit or implicit. In an explicit integration scheme, the yield surface, plastic potential gradients and hardening law are all evaluated at known stress states and no iteration is strictly necessary to predict the final stresses. Generally speaking, however, it is prudent to introduce a simple iterative correction to restore the final stresses and hardening parameters to the yield surface, as this condition is not enforced by the integration. In a fully implicit method, the gradients and hardening law are evaluated at unknown stress states and the resulting system of non-linear equations must be solved iteratively. If a Newton scheme is used for this purpose, then second derivatives of the yield function and plastic potential are required to implement the iteration. This can lead to much tedious algebra for complex soil plasticity models such as the critical state family (Schofield and Wroth, 1968). In practice, both implicit and explicit methods have been used to integrate advanced constitutive relations in soil mechanics (Borja and Lee, 1990; Borja, 1991; Potts and Gens, 1985; Britto and Gunn, 1987), but computational details of the schemes are seldom given.

Implicit methods are attractive because the resulting stresses automatically satisfy the yield criterion to a specified tolerance. Furthermore, they do not require the intersection with the yield surface to be computed if the stress point changes from an elastic state to a plastic state. A comprehensive discussion of various implicit integration schemes for elastoplastic models can be found in Ortiz and Simo (1986) and Crisfield (1991; 1997). One of the most popular of these is the backward Euler algorithm. This computes an elastic trial stress state, using either tangent elastic moduli or secant elastic moduli, and returns it back to the yield surface by closest-point projection iteration. In its most general form, the final stresses and hardening parameters are found by solving a small system of non-linear equations at each Gauss point. When using the Newton-Raphson algorithm for this task, care must be taken to allow for possible non-convergence of the resulting iteration scheme and some form of strain subincrementation may be necessary. The backward Euler return scheme has found wide application in metal plasticity studies since it provides all the information required for the formation of the consistent tangent stiffness matrix. This matrix, first identified by Simo and Taylor (1985), includes second order terms that are usually ignored in the standard form of the elastoplastic constitutive relations, and gives a quadratic rate of convergence for Newton-Raphson iteration of the global stiffness equations. Although powerful, the backward Euler return method is difficult to implement for complex constitutive relations because it requires second order derivatives of the yield function and plastic potential. Moreover, for yield surfaces with vertices or rapid changes in curvature, divergence may occur and it is advisable to use multi-vector return schemes (Crisfield, 1997). A discussion of various implicit integration methods for critical state models, including the backward Euler return scheme, can be found in Borja and Lee (1990) and Borja (1991).

Compared with implicit methods, explicit methods have the advantage of being more straightforward to implement. Since explicit schemes employ the standard elastoplastic constitutive law and require only first derivatives of the yield function and plastic potential, they can be used to design a general purpose integrator that can be used for a wide range of models. As discussed by Wissmann and Hauck (1983) and Sloan (1987), the accuracy and efficiency of explicit methods is significantly enhanced by combining them with automatic substepping and error control. Such schemes limit the error in the computed stresses with no intervention from the user, and are best employed in conjunction with a correction to restore the stresses to the yield surface during the integration process. Unlike implicit methods, explicit methods do not require the solution of a system of non-linear equations to compute the stresses at each Gauss point. They do, however, need to find the intermediate yield point if the stresses pass from an elastic state to a plastic state. This additional step only involves the solution of a single non-linear equation, but should be handled with care to avoid spurious intersections being found.

Somewhat surprisingly, few direct comparisons between explicit and explicit methods have been made in the literature. In two separate studies,

Potts and Ganendra (1992; 1994) compared the performance of the implicit return mapping algorithm of Ortiz and Simo (1986) with the explicit subincrementation scheme of Sloan (1987). For the modified Cam clay model, they concluded that the latter is more robust and efficient than the former. In another study, Yamaguchi (1993) compared explicit Runge-Kutta and forward Euler techniques with the implicit algorithm of Ortiz and Simo (1986) and found the Runge-Kutta scheme to be superior for problems with complicated constitutive laws or high accuracy demands. These conclusions are in general agreement with the experience of the authors.

The explicit substepping methods of Sloan (1987) were originally designed for conventional elastoplastic models where all deformation inside the yield surface is linear elastic and hardening is described by a single variable. In this paper, we extend these methods to cover generalised critical state models which exhibit non-linear elastic behaviour inside the yield surface. We also describe new intersection and stress correction algorithms that are general, robust and efficient. The integration algorithms use either a modified Euler scheme or a Runge-Kutta-Dormand-Prince scheme to estimate the local error in the computed stresses and control the subincrementation of the applied strain increment. The former scheme is suited to applications where moderate accuracy is needed and is the method of choice for most practical analyses. The latter scheme is more efficient for high accuracy work, and can be used to benchmark the accuracy of various integration schemes for complex constitutive relations. Detailed results are presented for the case of a smooth rigid footing resting on Tresca, Mohr-Coulomb, modified Cam clay and generalised Cam clay layers. For a given load path, we show that the modified Euler scheme is able to control the integration error to lie near a prescribed error tolerance. This feature is most attractive, as it permits the analyst to control the magnitude of the stress integration error in the overall solution process.

## 2. Stress-strain relations

During a typical step or iteration of an elastoplastic finite element analysis, the forces are applied in increments and the corresponding nodal displacement increments are found from the global stiffness equations. Once these displacements are known, the strain increments at a discrete number of integration points within each element are determined using the strain-displacement relations. If the stresses associated with an imposed strain increment cause plastic yielding, it is necessary to solve a small system of ordinary differential equations which may be written in the form:

$$\dot{\boldsymbol{\sigma}} = \mathbf{D}_{\text{ep}} \dot{\boldsymbol{\epsilon}}, \quad (1)$$

$$\dot{\mathcal{H}} = \dot{\lambda} B, \quad (2)$$

where  $\dot{\boldsymbol{\sigma}} = \{\dot{\sigma}_x, \dot{\sigma}_y, \dot{\sigma}_z, \dot{\tau}_{xy}, \dot{\tau}_{xz}, \dot{\tau}_{yz}\}^T$  is the stress rate vector,  $\dot{\boldsymbol{\epsilon}} = \{\dot{\epsilon}_x, \dot{\epsilon}_y, \dot{\epsilon}_z, \dot{\gamma}_{xy}, \dot{\gamma}_{xz}, \dot{\gamma}_{yz}\}^T$  is the strain rate vector,  $\dot{\mathcal{H}}$  is the rate of hardening parameter, and:

$$\begin{aligned}
 \mathbf{D}_{ep} &= \mathbf{D}_e - \frac{\mathbf{D}_e \mathbf{b} \mathbf{a}^T \mathbf{D}_e}{A + \mathbf{a}^T \mathbf{D}_e \mathbf{b}}, \\
 \mathbf{D}_e &= \begin{bmatrix} K + \frac{4}{3}G & K - \frac{2}{3}G & K - \frac{2}{3}G & 0 & 0 & 0 \\ & K + \frac{4}{3}G & K - \frac{2}{3}G & 0 & 0 & 0 \\ & & K + \frac{4}{3}G & 0 & 0 & 0 \\ \text{symm} & & & G & 0 & 0 \\ & & & & G & 0 \\ & & & & & G \end{bmatrix}, \\
 \dot{\lambda} &= \frac{\mathbf{a}^T \mathbf{D}_e \dot{\boldsymbol{\varepsilon}}}{A + \mathbf{a}^T \mathbf{D}_e \mathbf{b}}, \\
 A &= -\frac{\partial f}{\partial \mathcal{H}} \frac{\dot{\mathcal{H}}}{\dot{\lambda}}, \\
 B &= -\frac{A}{\partial f / \partial \mathcal{H}}, \\
 \mathbf{a} &= \frac{\partial f}{\partial \boldsymbol{\sigma}}, \\
 \mathbf{b} &= \frac{\partial g}{\partial \boldsymbol{\sigma}}.
 \end{aligned} \tag{3}$$

In the above,  $\mathbf{D}_{ep}$  denotes the elastoplastic stress-strain matrix,  $\mathbf{D}_e$  the elastic stress-strain matrix,  $K$  the elastic bulk modulus,  $G$  the shear modulus,  $f$  the yield function, and  $g$  the plastic potential.

In conventional elastoplastic constitutive laws the elastic moduli  $K$  and  $G$  (and hence the elastic stress-strain matrix  $\mathbf{D}_e$ ) are independent of the stresses and need to be computed only once. The precise form of the parameter  $A$  for these models depends on whether strain or work hardening is assumed and may usually be written in the form:

$$A = \begin{cases} -\frac{\partial f}{\partial \mathcal{H}} \sqrt{\frac{2}{3}} \mathbf{b}^T \mathbf{M} \mathbf{b} & \text{strain hardening,} \\ -\frac{\partial f}{\partial \mathcal{H}} \boldsymbol{\sigma}^T \mathbf{b} & \text{work hardening,} \end{cases}$$

where:

$$\mathbf{M} = \begin{bmatrix} 1 & & & & & \\ & 1 & & & & \\ & & 1 & & & \\ & & & 0.5 & & \\ & & & & 0.5 & \\ & & & & & 0.5 \end{bmatrix}.$$

For critical state models, the tangential bulk and shear moduli are often assumed to depend on the effective mean normal stress  $p'$  according to:

$$K = \frac{\partial p'}{\partial \varepsilon_v^e} = \frac{1+e}{k} p' = \frac{vp'}{k}, \quad (4)$$

$$G = \frac{3(1-2\mu)K}{2(1+\mu)} = \frac{3(1-2\mu)}{2(1+\mu)} \frac{vp'}{k}, \quad (5)$$

where  $\varepsilon_v^e$  is the elastic volumetric strain,  $e$  is the void ratio,  $k$  is the slope of the unload/reload line on a  $\ln p' - v$  plot,  $v$  is the specific volume and  $\mu$  is Poisson's ratio. The stress dependence of  $K$  and  $G$  means that the stress-strain matrix  $\mathbf{D}_e$  is in fact non-linear elastic and no purely elastic behaviour exists. Integrating equation (4) for  $p'$  and  $\varepsilon_v^e$  results in the secant bulk modulus:

$$\bar{K} = \frac{p'_0}{\Delta \varepsilon_v^e} (\exp(v \Delta \varepsilon_v^e / k) - 1), \quad (6)$$

where  $p'_0$  is the effective mean normal stress at the start of the strain increment  $\Delta \varepsilon_v^e$ . Assuming Poisson's ratio is constant, the secant shear modulus can be computed from equation (5) as:

$$\bar{G} = \frac{3(1-2\mu)\bar{K}}{2(1+\mu)}. \quad (7)$$

These secant moduli are used to find accurate trial stress states for various integration algorithms and, in the case of an explicit scheme, are essential to compute the correct intersection with the yield surface when a stress point passes from an elastic state to a plastic state.

Various methods for smoothing the vertices in Tresca and Mohr-Coulomb yield functions have been discussed by Abbo (1997). These provide a simple and efficient means for avoiding singularities in the elastoplastic stress-strain relations, as they permit the gradient vectors  $\mathbf{a}$  and  $\mathbf{b}$  to be computed for any stress state. Critical state models may assume a variety of forms for the yield surface, the plastic potential, and the failure surface in the deviatoric plane (Schofield and Wroth, 1968; Randolph, 1982; Roscoe and Burland, 1968; Lade and Duncan, 1975; Van Eekelen, 1980; Naylor, 1985). Roscoe and Burland (1968), for example, suggest that the von Mises yield surface should be used together with a Mohr-Coulomb failure criterion. Here we assume a generalised Cam clay yield function with an associated flow rule of the form:

$$f - g = \frac{1}{\beta^2} \left( \frac{(1+\beta')p'}{p'_0} - 1 \right)^2 + \left( \frac{(1+\beta')q}{M(\theta)p'_0} \right)^2 - 1, \quad (8)$$

where  $q$  is the deviator stress,  $M(\theta)$  is the slope of the critical state line (CSL) in the  $p' - q$  plane,  $\theta$  is the Lode angle,  $p'_0$  is the isotropic preconsolidation pressure,

and  $\alpha$  and  $(\beta, \beta')$  are parameters which control the shape of the yield surface in the  $p'$ - $q$  and deviatoric planes respectively (Figure 1). On the dry side of the critical state line  $\beta = 1$ , while on the wet side  $\beta = \beta'$ . The variation of  $M$  with the Lode angle in equation (8) follows the relation proposed by Sheng *et al.* (1999) according to:

$$M(\theta) = M_{\max} \left( \frac{2\alpha^4}{1 + \alpha^4 - (1 - \alpha^4) \sin 3\theta} \right)^{1/4},$$

where  $M_{\max}$  is the slope of the CSL under triaxial compression ( $\theta = 30^\circ$ ). If  $\phi'$  denotes the friction angle of the soil at critical state, we can generate a surface which approximates the Mohr-Coulomb surface in the deviatoric plane by setting  $\alpha = (3 - \sin \phi') / (3 + \sin \phi')$ .

The hardening law for critical state models is usually described by a rate relation between the volumetric plastic strain  $\varepsilon_v^e$  and the isotropic preconsolidation pressure  $p'_0$  according to:

$$\dot{\varepsilon}_v^p = \frac{\lambda - k}{vp'_0} \dot{p}'_0, \quad (9)$$

where  $\lambda$  is the slope of the normal compression line in a  $\ln p'$ - $v$  plot. Assuming the hardening parameter  $\mathcal{H}$  is equal to  $p'_0$  and substituting equation (9) into equation (6) we obtain:

$$A = \frac{\partial f}{\partial \mathcal{H}} \frac{\dot{\mathcal{H}}}{\dot{\lambda}} = -\frac{vp'_0}{\lambda - k} \frac{\partial f}{\partial p'_0} \frac{\dot{\varepsilon}_v^p}{\dot{\lambda}} = -\frac{vp'_0}{\lambda - k} \frac{\partial f}{\partial p'_0} \frac{\partial g}{\partial p'},$$

which implies that:

$$B = -\frac{A}{\partial f / \partial \mathcal{H}} = \frac{vp'_0}{\lambda - k} \frac{\partial g}{\partial p'}. \quad (10)$$

To integrate equations (1) and (2) numerically, it is convenient to introduce a pseudo time,  $T$ , defined by:

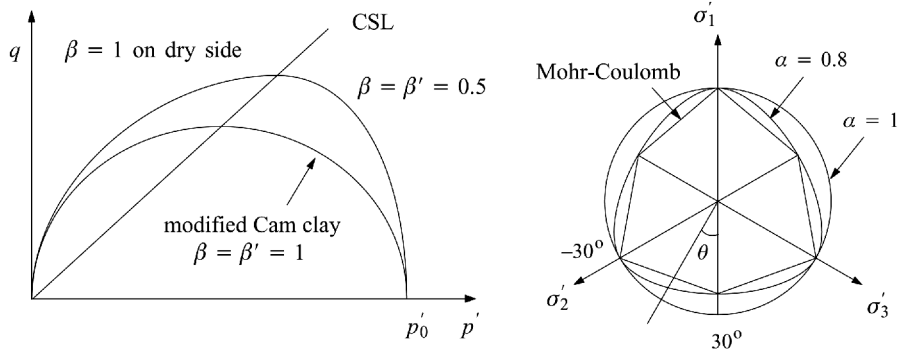


**Figure 1.**  
Generalised critical state model in the  $p'$ - $q$  and deviatoric planes

$$T = (t - t_0)/\Delta t,$$

where  $t_0$  is the time at the start of the load increment,  $t_0 + \Delta t$  is the time at the end of the load increment, and  $0 \leq T \leq 1$ . Since  $dT/dt = 1/\Delta t$ , application of the chain rule to  $\dot{\boldsymbol{\sigma}}$  and  $\dot{\mathcal{H}}$  in equations (1) and (2) gives:

$$\frac{d\boldsymbol{\sigma}}{dT} = \mathbf{D}_{\text{ep}}\Delta\boldsymbol{\epsilon} = \left( \mathbf{D}_e - \frac{\mathbf{D}_e\mathbf{b}\mathbf{a}^T\mathbf{D}_e}{A + \mathbf{a}^T\mathbf{D}_e\mathbf{b}} \right) \Delta\boldsymbol{\epsilon} = \Delta\boldsymbol{\sigma}_e - \Delta\lambda\mathbf{D}_e\mathbf{b}, \quad (11)$$

127

$$\frac{d\mathcal{H}}{dT} = \dot{\lambda}\Delta t B = \Delta\lambda B, \quad (12)$$

where:

$$\Delta\lambda = \frac{\mathbf{a}^T\mathbf{D}_e\Delta\boldsymbol{\epsilon}}{A + \mathbf{a}^T\mathbf{D}_e\mathbf{b}} = \frac{\mathbf{a}^T\Delta\boldsymbol{\sigma}_e}{A + \mathbf{a}^T\mathbf{D}_e\mathbf{b}}.$$

Note that, in keeping with the philosophy of the static displacement finite element procedure, the strain rate is assumed to be constant and equal to  $\Delta\boldsymbol{\epsilon}/\Delta t$ . Equations (11) and (12) define a classical initial value problem to be integrated over the pseudo time interval  $T = 0$  to  $T = 1$ . The known values in these relations are the imposed strain increments,  $\Delta\boldsymbol{\epsilon}$ , together with the stresses and hardening parameter at the start of the pseudo time increment.

### 3. Explicit integration schemes

The substepping algorithms of Sloan (1987) integrate the constitutive law by automatically dividing the strain increment into a number of substeps. An appropriate size for each substep is found through the use of modified Euler or higher order Runge-Kutta formulae, which are specially constructed to provide an estimate of the local error. The performance of a variety of these schemes for Tresca and Mohr-Coulomb elastoplastic models, under plane strain conditions, has been considered in detail by Sloan and Booker (1992).

The explicit substepping schemes described here are based on the algorithms of Sloan (1987) but include a number of important enhancements to improve their accuracy, efficiency and robustness. In particular, Sloan's original procedures are generalised to cover non-linear elastic behaviour and incorporate new algorithms for handling elastoplastic unloading, computing the yield intersection point, and restoring the stresses to the yield surface. Each of these aspects is now described in more detail.

#### 3.1 Yield surface intersection

Given a vector of imposed strain increments  $\Delta\boldsymbol{\epsilon}$ , an elastic trial stress increment  $\Delta\boldsymbol{\sigma}_e$  can be found using Hooke's law according to:

$$\Delta\boldsymbol{\sigma}_e = \mathbf{D}_e\Delta\boldsymbol{\epsilon}. \quad (13)$$

If the elastic part of the constitutive relation is linear, the stress-strain matrix  $\mathbf{D}_e$  is independent of the stresses and it is trivial to compute the elastic trial state  $\boldsymbol{\sigma}_e = \boldsymbol{\sigma}_0 + \Delta\boldsymbol{\sigma}_e$  (where  $\boldsymbol{\sigma}_0$  is the initial stress state). For non-linear elastic behaviour, however, the above equation must in general be integrated to compute the proper value of  $\Delta\boldsymbol{\sigma}_e$ . In critical state elasticity, the incremental relation between the mean stress and the elastic volumetric strain can be integrated analytically to give the secant elastic moduli defined by equations (6) and (7). This permits the corresponding secant elastic stiffness matrix  $\overline{\mathbf{D}}_e$ , defined by  $\overline{K}$  and  $\overline{G}$ , to be formed and the relation (13) is replaced by:

$$\Delta\overline{\boldsymbol{\sigma}}_e = \overline{\mathbf{D}}_e(\overline{K}, \overline{G})\Delta\boldsymbol{\varepsilon} = \overline{\mathbf{D}}_e(\boldsymbol{\sigma}_0, \Delta\varepsilon_v)\Delta\boldsymbol{\varepsilon} = \overline{\mathbf{D}}_e\Delta\boldsymbol{\varepsilon}.$$

In this equation,  $\overline{K}$  and  $\overline{G}$  are evaluated using the initial stress state  $\boldsymbol{\sigma}_0$  and the total volumetric strain increment  $\Delta\varepsilon_v$ . For the linear elasticity that occurs in conventional plasticity models, the trial stress increment  $\Delta\boldsymbol{\sigma}_e$  can be used later in the stress integration procedure. For non-linear critical state elasticity, however, the elastic trial stress increment  $\Delta\overline{\boldsymbol{\sigma}}_e$  is used only to check if the stress state has changed from elastic to plastic. Such a change occurs if  $f(\boldsymbol{\sigma}_0, \mathcal{H}_0) < 0$  and  $f(\boldsymbol{\sigma}_0 + \Delta\overline{\boldsymbol{\sigma}}_e, \mathcal{H}_0) = f(\overline{\boldsymbol{\sigma}}_e, \mathcal{H}_0) > 0$ , and it is then necessary to ascertain the fraction of  $\Delta\boldsymbol{\varepsilon}$  that moves the stresses from  $\boldsymbol{\sigma}_0$  to the stress state  $\boldsymbol{\sigma}_{\text{int}}$  on the yield surface. This situation, shown in Figure 2, may arise many times during the course of an elastoplastic finite element analysis and needs to be handled efficiently and accurately. Note that in Figure 2 the exact yield condition  $f(\boldsymbol{\sigma}, \mathcal{H}) = 0$  is replaced by the approximation  $|f(\boldsymbol{\sigma}, \mathcal{H})| \leq FTOL$ , where  $FTOL$  is a small positive tolerance. This allows for the effects of finite precision arithmetic and modifies the transition condition to  $f(\boldsymbol{\sigma}_0, \mathcal{H}_0) < -FTOL$  and  $f(\overline{\boldsymbol{\sigma}}_e, \mathcal{H}_0) > +FTOL$ . Suitable values for the yield surface tolerance are typically in the range  $10^{-6}$  to  $10^{-9}$ .

The problem of finding the stresses at the yield surface intersection point  $\boldsymbol{\sigma}_{\text{int}}$  is equivalent to finding the scalar quantity  $\alpha$  which satisfies the non-linear equation:

$$f(\boldsymbol{\sigma}_0 + \alpha\overline{\mathbf{D}}_e\Delta\boldsymbol{\varepsilon}, \mathcal{H}_0) = f(\boldsymbol{\sigma}_{\text{int}}, \mathcal{H}_0) = 0. \quad (14)$$

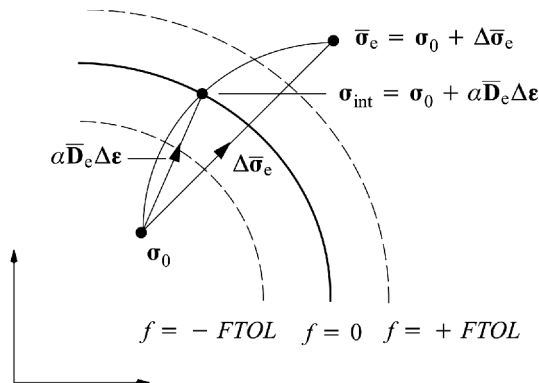


**Figure 2.**  
Yield surface  
intersection: elastic to  
plastic transition

A value of  $\alpha = 0$  indicates that  $\Delta\boldsymbol{\varepsilon}$  causes purely plastic deformation, while a value of  $\alpha = 1$  indicates purely “elastic” deformation. Thus, for an elastic to plastic transition, we have  $0 < \alpha < 1$  and the “elastic” part of the stress increment is given by  $\alpha\overline{\mathbf{D}}_e\Delta\boldsymbol{\varepsilon}$ . For critical state models, the secant elastic stress-strain matrix  $\overline{\mathbf{D}}_e$  is evaluated using the initial stress  $\boldsymbol{\sigma}_0$  and the strain increment  $\alpha\Delta\boldsymbol{\varepsilon}$ . This means the trial elastic stress state, for a given initial stress and imposed strain increment, is exact and leads to accurate estimates of the intersection stress  $\boldsymbol{\sigma}_{\text{int}}$ .

Equation (14) defines a single non-linear equation in the variable  $\alpha$  and can be solved by a variety of numerical methods including the bisection, regula-falsi, modified regula-falsi, secant, and Newton-Raphson schemes (see, for example, Conte and de Boor (1980) for a detailed discussion of these). The first three algorithms are unconditionally convergent for continuous yield functions and confine the solution for  $\alpha$  to lie within specified bounds. They are, however, sometimes slow to converge for cases where  $df/d\alpha$  is large. The Newton-Raphson and secant techniques offer rapid convergence rates but may diverge in some circumstances because they do not constrain the solution for  $\alpha$  to lie within specified bounds. The Pegasus procedure of Dowell and Jarratt (1972) is ideally suited to solving the yield surface intersection problem defined by equation (14) since it is unconditionally convergent, does not require the use of derivatives, and typically converges in four or five iterations (even when used with stringent values for the tolerance  $FTOL$ ).

The complete Pegasus algorithm is detailed below.

*Pegasus intersection scheme for critical state models:*

- (1) Enter with stresses  $\boldsymbol{\sigma}_0$  and hardening parameter  $\mathcal{H}_0$ , the strain increment  $\Delta\boldsymbol{\varepsilon}$ , initial values of  $\alpha_0$  and  $\alpha_1$  bounding the intersection with the yield surface, and the maximum number of iterations  $MAXITS$ .
- (2) Calculate:
 
$$\begin{aligned}\overline{\mathbf{D}}_{e0} &= \overline{\mathbf{D}}_e(\boldsymbol{\sigma}_0, \alpha_0\Delta\varepsilon_v), \\ \Delta\overline{\boldsymbol{\sigma}}_{e0} &= \alpha_0\overline{\mathbf{D}}_{e0}\Delta\boldsymbol{\varepsilon}, \\ \overline{\mathbf{D}}_{e1} &= \overline{\mathbf{D}}_e(\boldsymbol{\sigma}_0, \alpha_1\Delta\varepsilon_v), \\ \Delta\overline{\boldsymbol{\sigma}}_{e1} &= \alpha_1\overline{\mathbf{D}}_{e1}\Delta\boldsymbol{\varepsilon}.\end{aligned}$$
- (3) Set  $F_0 = f(\boldsymbol{\sigma}_0 + \Delta\overline{\boldsymbol{\sigma}}_{e0}, \mathcal{H}_0)$  and  $F_1 = f(\boldsymbol{\sigma}_0 + \Delta\overline{\boldsymbol{\sigma}}_{e1}, \mathcal{H}_0)$ .
- (4) Perform steps 5-8  $MAXITS$  times.
- (5) Calculate:
 
$$\alpha = \alpha_1 - F_1 \times (\alpha_1 - \alpha_0) / (F_1 - F_0),$$
 and set:
 
$$\begin{aligned}\overline{\mathbf{D}}_e &= \overline{\mathbf{D}}_e(\boldsymbol{\sigma}_0, \alpha\Delta\varepsilon_v), \\ \Delta\overline{\boldsymbol{\sigma}}_e &= \alpha\overline{\mathbf{D}}_e\Delta\boldsymbol{\varepsilon}, \\ F_{\text{new}} &= f(\boldsymbol{\sigma}_0 + \Delta\overline{\boldsymbol{\sigma}}_e, \mathcal{H}_0).\end{aligned}$$
- (6) If  $|F_{\text{new}}| \leq FTOL$  go to step 10.
- (7) If  $F_{\text{new}}$  is of the opposite sign to  $F_0$  then:
 
$$\text{Set } \alpha_1 = \alpha \text{ and } F_1 = F_{\text{new}},$$

else:  
Set  $F_1 = F_1 F_0 / (F_0 F_{\text{new}})$ .

- (8) Set  $\alpha_0 = \alpha$  and  $F_0 = F_{\text{new}}$ .
- (9) Convergence not achieved after *MAXITS* iterations, print error message and stop.
- (10) Exit with  $\alpha$ .

For conventional elastoplastic models, where the elastic stress-strain matrix is constant, the elastic trial stress needs to be calculated only once. This means that steps 2, 3 and 5 of the Pegasus algorithm simplify to the following.

*Pegasus intersection scheme for conventional elastoplastic models:*

- (2) Calculate:  
$$\Delta \boldsymbol{\sigma}_e = \mathbf{D}_e \Delta \boldsymbol{\varepsilon}.$$
- (3) Set  $F_0 = f(\boldsymbol{\sigma}_0 + \alpha_0 \Delta \boldsymbol{\sigma}_e, \mathcal{H}_0)$  and  $F_1 = f(\boldsymbol{\sigma}_0 + \alpha_1 \Delta \boldsymbol{\sigma}_e, \mathcal{H}_0)$ .
- (5) Calculate:  
$$\alpha = \alpha_1 - F_1 \times (\alpha_1 - \alpha_0) / (F_1 - F_0),$$
  
and set:  
$$F_{\text{new}} = f(\boldsymbol{\sigma}_0 + \alpha \Delta \boldsymbol{\sigma}_e, \mathcal{H}_0).$$

In the absence of better information, the algorithms above are started by specifying  $\alpha_0 = 0$  and  $\alpha_1 = 1$ . The maximum number of iterations permitted, *MAXITS*, is typically set to ten and the procedure is terminated once the intersection stresses satisfy the condition  $|f(\boldsymbol{\sigma}_{\text{int}}, \mathcal{H}_0)| \leq FTOL$ .

### 3.2 Elastoplastic unloading

An elastic to plastic transition may also occur if a stress point, initially lying on the yield surface, is subject to an elastoplastic stress increment of the type shown in Figure 3. This situation arises when the the angle  $\theta$  between the yield

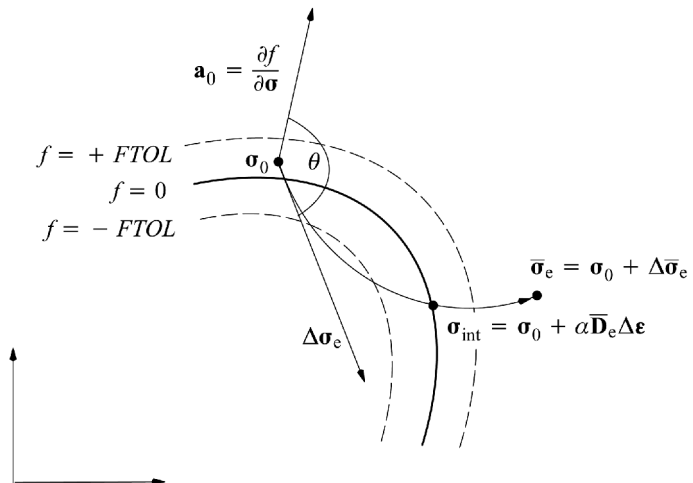


**Figure 3.**  
Yield surface  
intersection:  
elastoplastic unloading

surface gradient  $\mathbf{a}_0$  and the tangential elastic stress increment  $\Delta\boldsymbol{\sigma}_e$  is larger than  $90^\circ$  and  $f(\bar{\boldsymbol{\sigma}}_e, \mathcal{H}_0) > +FTOL$ . The first of these conditions may be written as:

$$\cos \theta = \frac{\mathbf{a}_0^T \Delta\boldsymbol{\sigma}_e}{\|\mathbf{a}_0\|_2 \|\Delta\boldsymbol{\sigma}_e\|_2} < -LTOL,$$

where  $\mathbf{a}_0$  is evaluated at the initial stress state  $\boldsymbol{\sigma}_0$ ,  $\Delta\boldsymbol{\sigma}_e$  is computed using the elastic tangential moduli, and  $LTOL$  is a suitable tolerance. This type of stress path can occur near the tip of a failure surface if  $\Delta\bar{\boldsymbol{\sigma}}_e$  is large owing to the use of discrete load increments, and does not require unloading of the overall structure. Because the portion of the stress path inside the yield surface is “elastic” and can be integrated exactly (using the secant elastic moduli), the elastoplastic constitutive law need only be integrated numerically beyond the last intersection point.

The procedure for finding the yield surface intersection for elastoplastic unloading is the same as discussed in section 3.1, though a different set of starting values for  $\alpha$  must be used. The situation is complicated by the fact that the stress increment may cross the yield surface twice, as shown in Figure 4. This possibility is caused by the use of the tolerance  $FTOL$ , which permits the stresses to lie just outside the yield surface, and must be properly accounted for. To ensure the Pegasus algorithm finds the correct crossing, it is sufficient to determine starting values,  $\alpha_0$  and  $\alpha_1$ , which satisfy  $f(\boldsymbol{\sigma}_0 + \alpha_0 \bar{\mathbf{D}}_e \Delta\boldsymbol{\epsilon}, \mathcal{H}_0) < -FTOL$  and  $f(\boldsymbol{\sigma}_0 + \alpha_1 \bar{\mathbf{D}}_e \Delta\boldsymbol{\epsilon}, \mathcal{H}_0) > FTOL$ . Ignoring multiple roots, which have not been observed in practice, these conditions guarantee that  $\alpha_0$  and  $\alpha_1$  bracket the second yield surface intersection. As in the previous case,  $\alpha = 0$  indicates the strain increment  $\Delta\boldsymbol{\epsilon}$  causes purely plastic deformation while  $\alpha = 1$  indicates purely elastic deformation. Because we assume that  $f(\bar{\boldsymbol{\sigma}}_e, \mathcal{H}) > FTOL$ ,  $\alpha$  again must lie within the range  $0 < \alpha < 1$ .

One crude but successful strategy for finding values which bracket the desired crossing involves breaking up the strain increment  $\Delta\boldsymbol{\epsilon}$  into a number of smaller subincrements. The number of subincrements used in the search,  $NSUB$ , is typically set to ten, although numerical experiments suggest that as few as two subincrements may be used with only a marginal increase in computation time. In the first iteration of the algorithm, the subincrement

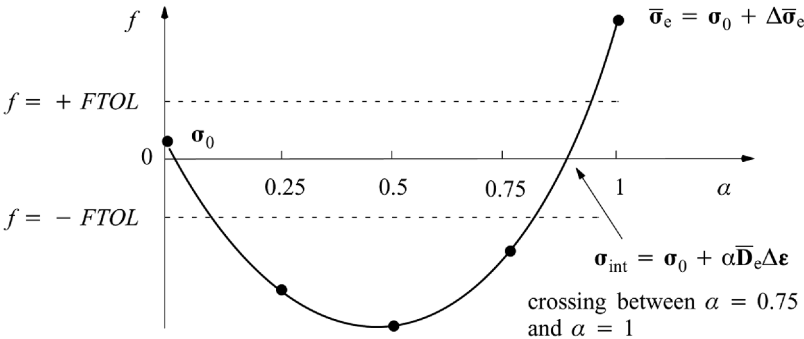


**Figure 4.** Starting values for yield surface intersection: elastoplastic unloading

size is set to  $\Delta\boldsymbol{\varepsilon}/NSUB$  (which corresponds to subincrements in  $\alpha$  of  $\Delta\alpha = 1/NSUB$ ). A check is then made to see if a crossing lies in any of the intervals defined by the pairs  $(\alpha_{n-1}, \alpha_n)$ , where  $\alpha_n = \alpha_{n-1} + n\Delta\alpha$ ,  $\alpha_0 = 0$ , and  $n = 1, 2, \dots, NSUB$ . Such a crossing takes place if  $f(\boldsymbol{\sigma}_0 + \alpha_{n-1}\overline{\mathbf{D}}_e\Delta\boldsymbol{\varepsilon}, \mathcal{H}_0) < -FTOL$  and  $f(\boldsymbol{\sigma}_0 + \alpha_n\overline{\mathbf{D}}_e\Delta\boldsymbol{\varepsilon}, \mathcal{H}_0) > FTOL$ . A geometric illustration of a successful search with four subincrements is shown in Figure 4. In this example the required intersection with the yield surface lies between  $\alpha = 0.75$  and  $\alpha = 1$ , and these two limits serve as good starting values for the Pegasus search.

If the strain increment  $\Delta\boldsymbol{\varepsilon}$  is very large, or the stress increment  $\Delta\overline{\boldsymbol{\sigma}}_e$  is nearly tangent to the yield surface, the initial subincrement size may not be small enough to detect the required crossing. Although rare, this case can be checked by testing if  $f(\boldsymbol{\sigma}_0 + \alpha_{n-1}\overline{\mathbf{D}}_e\Delta\boldsymbol{\varepsilon}, \mathcal{H}_0) \geq -FTOL$  and  $f(\boldsymbol{\sigma}_0 + \alpha_n\overline{\mathbf{D}}_e\Delta\boldsymbol{\varepsilon}, \mathcal{H}_0) > FTOL$  for each pair of values  $(\alpha_{n-1}, \alpha_n)$ . If these two conditions are true, the crossing lies in the interval  $(0, \alpha_n)$  and the search can be restarted using a smaller subincrement size of  $\Delta\alpha = \alpha_n/NSUB$ . Because each restart gives a diminishing benefit, they are usually limited in number.

Using the above strategy, the yield surface intersection point for elastoplastic unloading with a critical state model may be found as follows.

*Pegasus scheme for elastoplastic unloading with a critical state model:*

- (1) Enter with initial stresses  $\boldsymbol{\sigma}_0$ , initial hardening parameter  $\mathcal{H}_0$ , and strain increment  $\Delta\boldsymbol{\varepsilon}$ .
- (2) Set  $\alpha_0 = 0$ ,  $\alpha_1 = 1$ ,  $F_0 = f(\boldsymbol{\sigma}_0, \mathcal{H}_0)$ , and  $F_{\text{save}} = F_0$ .
- (3) Perform steps 4 and 5 *MAXITS* times.
- (4) Calculate:  
$$\Delta\alpha = (\alpha_1 - \alpha_0)/NSUB.$$
- (5) Perform steps 6 and 7 *NSUB* times
- (6) Calculate:  
$$\overline{\mathbf{D}}_e = \overline{\mathbf{D}}_e(\boldsymbol{\sigma}_0, \alpha\Delta\varepsilon_v),$$
  
$$\Delta\overline{\boldsymbol{\sigma}}_e = \overline{\mathbf{D}}_e\alpha\Delta\boldsymbol{\varepsilon},$$
  
$$\boldsymbol{\sigma}_1 = \boldsymbol{\sigma}_0 + \Delta\overline{\boldsymbol{\sigma}}_e,$$
  
where:  
$$\alpha = \alpha_0 + \Delta\alpha.$$
- (7) If  $f(\boldsymbol{\sigma}_1, \mathcal{H}_0) > FTOL$ , then:  
Set  $\alpha_1 = \alpha$   
If  $F_0 < -FTOL$ ,  
set  $F_1 = f(\boldsymbol{\sigma}_1, \mathcal{H}_0)$  and go to step 9.  
else  
set  $\alpha_0 = 0$  and  $F_0 = F_{\text{save}}$  and exit loop over steps 6 and 7.  
else  
set  $\alpha_0 = \alpha$  and  $F_0 = f(\boldsymbol{\sigma}_1, \mathcal{H}_0)$ .

- (8) Intersection not found after *MAXITS* iterations, print error message and stop.
- (9) Exit with  $\alpha_0$  and  $\alpha_1$  bounding the yield surface intersection.
- (10) Call the Pegasus algorithm with  $\alpha_0$  and  $\alpha_1$  to locate the yield surface intersection.

For a conventional elastoplastic model with a constant elastic stress-strain matrix, steps 1 and 6 of the above algorithm can be made more efficient as follows.

*Pegasus scheme for elastoplastic unloading with a conventional elastoplastic model:*

- (1) Enter with initial stresses  $\boldsymbol{\sigma}_0$ , initial hardening parameter  $\mathcal{H}_0$ , and elastic stress increment  $\Delta\boldsymbol{\sigma}_e = \mathbf{D}_e\Delta\boldsymbol{\epsilon}$ .
- (6) Calculate:
 
$$\boldsymbol{\sigma}_1 = \boldsymbol{\sigma}_0 + \alpha\Delta\boldsymbol{\sigma}_e,$$
 where:
 
$$\alpha = \alpha_0 + \Delta\alpha.$$

Typically, the number of subincrements, *NSUB*, is set to ten while the maximum number of restart iterations, *MAXITS*, is set to three.

### 3.3 Correction of stresses to yield surface

At the end of each subincrement in the explicit integration process, the stresses may diverge from the yield condition so that  $|f(\boldsymbol{\sigma}, \mathcal{H})| > FTOL$ . The extent of this violation, which is commonly known as yield surface “drift”, depends on the accuracy of the integration scheme and the non-linearity of the constitutive relations. In his original study Sloan (1987) suggested that, provided the integration is performed accurately, the amount of yield surface drift will be small and any remedial action is optional. Others, including Potts and Gens (1985) and Crisfield (1991), strongly advocate some form of iterative stress correction as the effects of violating the yield condition are cumulative. The numerical experience of the authors suggests it is indeed prudent to impose a yield surface correction at the end of each subincrement, especially for complicated constitutive models such as the critical state family. In this section, we describe an efficient and robust combination of two different methods for restoring the stresses to the yield surface.

Consider a point where the uncorrected stresses and hardening parameter, defined by  $\boldsymbol{\sigma}_0$  and  $\mathcal{H}_0$ , violate the yield condition so that  $|f(\boldsymbol{\sigma}_0, \mathcal{H}_0)| > FTOL$ . Ignoring second order terms and above,  $f$  may be expanded in a Taylor series about this stress point to give:

$$f = f_0 + \mathbf{a}_0^T \delta\boldsymbol{\sigma} + \frac{\partial f}{\partial \mathcal{H}} \delta\mathcal{H}, \quad (15)$$

where  $\delta\boldsymbol{\sigma}$  is a small stress correction,  $\delta\mathcal{H}$  is a small hardening parameter correction,  $f_0 = f(\boldsymbol{\sigma}_0, \mathcal{H}_0)$ , and  $\mathbf{a}_0$  is evaluated at  $\boldsymbol{\sigma}_0$ . In returning the stress state to the yield surface, it is desirable that the total strain increment  $\Delta\boldsymbol{\epsilon}$  remains unchanged, since this is consistent with the philosophy of the displacement finite element procedure (Potts and Gens, 1985). From equation (11), we see the imposed strain increments remain unchanged provided the stress correction obeys the relation:

$$\delta\boldsymbol{\sigma} = -\delta\lambda\mathbf{D}_e\mathbf{b}_0, \quad (16)$$

where  $\delta\lambda$  is an unknown multiplier and  $\mathbf{b}_0$  is evaluated at  $\boldsymbol{\sigma}_0$ . Using equation (2), the corresponding hardening correction is:

$$\delta\mathcal{H} = \delta\lambda B_0 = -\delta\lambda \frac{A_0}{df/d\mathcal{H}}, \quad (17)$$

where  $A_0$  and  $B_0$  are evaluated at  $\boldsymbol{\sigma}_0$ . Combining equations (15)-(17) and setting  $f = 0$  gives the unknown multiplier as:

$$\delta\lambda = f_0 / (A_0 + \mathbf{a}_0^T \mathbf{D}_e \mathbf{b}_0).$$

The corrections to the stresses and hardening parameter are thus given by:

$$\begin{aligned} \delta\boldsymbol{\sigma} &= -f_0 \mathbf{D}_e \mathbf{b}_0 / (A_0 + \mathbf{a}_0^T \mathbf{D}_e \mathbf{b}_0), \\ \delta\mathcal{H} &= f_0 B_0 / (A_0 + \mathbf{a}_0^T \mathbf{D}_e \mathbf{b}_0), \end{aligned}$$

and an improved stress state, which is closer to the yield surface, can be obtained from:

$$\begin{aligned} \boldsymbol{\sigma} &= \boldsymbol{\sigma}_0 + \delta\boldsymbol{\sigma}, \\ \mathcal{H} &= \mathcal{H}_0 + \delta\mathcal{H}. \end{aligned}$$

This type of scheme, which is known as a consistent correction, may be applied repeatedly until  $|f(\boldsymbol{\sigma}, \mathcal{H})| \leq FTOL$ . It has been used successfully for critical state soil models by Potts and Gens (1985) and is also advocated by Crisfield (1991). Under certain conditions, such as those that occur near the tip of the Mohr-Coulomb yield surface for a material with a non-associated flow rule, this technique may not converge. Non-convergent behaviour is usually signalled when the corrected stress state is further from the yield surface than the uncorrected stress state. In these circumstances, the consistent return scheme may be abandoned for one iteration and replaced with a correction which is normal to the yield surface. The latter method, which we term a normal correction, does not preserve the total applied strain increment but is robust and has been used successfully by Nayak and Zienkiewicz (1972), Owen and Hinton (1980) and Sloan and Randolph (1982). With the normal correction scheme, equation (16) is replaced by:

$$\delta \boldsymbol{\sigma} = -\delta \lambda \mathbf{a}_0,$$

and it is assumed that the hardening parameter  $\mathcal{H}_0$  remains unchanged. Using the same argument as before, but neglecting any changes in  $\mathcal{H}$ , it follows that:

$$\delta \boldsymbol{\sigma} = -f_0 \mathbf{a}_0 / (\mathbf{a}_0^T \mathbf{a}_0). \quad (18)$$

This type of correction may also be applied iteratively until  $|f(\boldsymbol{\sigma}, \mathcal{H}_0)| \leq FTOL$ .

The complete algorithm for returning the stresses to the yield surface and may be summarised as follows.

*Yield surface correction scheme for general elastoplastic models:*

- (1) Enter with uncorrected stresses  $\boldsymbol{\sigma}_0$  and hardening parameter  $\mathcal{H}_0$ .
- (2) Perform steps 3-6 *MAXITS* times.
- (3) Compute:
 
$$\delta \lambda = f_0 / (A_0 + \mathbf{a}_0^T \mathbf{D}_e \mathbf{b}_0),$$
 and then correct stresses and hardening parameter using:
 
$$\boldsymbol{\sigma} = \boldsymbol{\sigma}_0 - \delta \lambda \mathbf{D}_e \mathbf{b}_0,$$

$$\mathcal{H} = \mathcal{H}_0 + \delta \lambda B_0.$$
- (4) If  $|f(\boldsymbol{\sigma}, \mathcal{H})| > |f(\boldsymbol{\sigma}_0, \mathcal{H}_0)|$ , then abandon previous correction and compute:
 
$$\delta \lambda = f_0 / (\mathbf{a}_0^T \mathbf{a}_0),$$

$$\boldsymbol{\sigma} = \boldsymbol{\sigma}_0 - \delta \lambda \mathbf{a}_0,$$

$$\mathcal{H} = \mathcal{H}_0.$$
- (5) If  $|f(\boldsymbol{\sigma}, \mathcal{H})| \leq FTOL$ , then go to step 8.
- (6) Set  $\boldsymbol{\sigma}_0 = \boldsymbol{\sigma}$  and  $\mathcal{H}_0 = \mathcal{H}$ .
- (7) Convergence not achieved after *MAXITS* steps, print error message and stop.
- (8) Exit with stresses  $\boldsymbol{\sigma}$  and hardening parameter  $\mathcal{H}$  lying on the yield surface.

A suitable value for *MAXITS*, the maximum number of correction iterations permitted, is typically between five and ten. *FTOL* may be set anywhere in the range  $10^{-6}$ - $10^{-12}$ , with the larger value being acceptable for most practical situations.

### 3.4 Modified Euler scheme with substepping

For a given strain increment,  $\Delta \boldsymbol{\varepsilon}$ , the constitutive relations to be integrated at each Gauss point are described by equations (11) and (12) as:

$$\frac{d\boldsymbol{\sigma}}{dT} = \mathbf{D}_{ep} \Delta \boldsymbol{\varepsilon} = \Delta \boldsymbol{\sigma}_e - \Delta \lambda \mathbf{D}_e \mathbf{b}, \quad (19)$$

$$\frac{d\mathcal{H}}{dT} = \Delta\lambda B, \quad (20)$$

where:

$$\Delta\lambda = \frac{\mathbf{a}^T \mathbf{D}_e \Delta\boldsymbol{\epsilon}}{A + \mathbf{a}^T \mathbf{D}_e \mathbf{b}},$$

and the pseudo time lies in the range:

$$0 \leq T \leq 1.$$

These equations describe a system of ordinary differential equations with initial conditions  $\boldsymbol{\sigma} = \boldsymbol{\sigma}_0$  and  $\mathcal{H} = \mathcal{H}_0$  at the start of the increment where  $T = 0$  and  $t = t_0$ . A wide variety of explicit integration methods may be used to find the stresses and hardening parameter at the end of the increment (where  $T = 1$ ), but we will focus on the approach first proposed by Sloan (1987). This method is attractive for finite element applications because it attempts to control the errors in the stresses and hardening parameter arising from the approximate integration of the constitutive law. Following a practice that is used widely to solve ordinary differential equations, the error control is achieved by using a local error measure to automatically subincrement the imposed strain increment  $\Delta\boldsymbol{\epsilon}$ . For each subincrement, the local error measure is found by taking the difference between a second order accurate modified Euler solution and a first order accurate Euler solution. Once the local error has been computed for a given step, the size of the next step is determined using an expression for the dominant error term. This type of error control permits the size of each subincrement to vary throughout the integration process, depending on the non-linearity of the constitutive relations.

Consider a pseudo time subincrement in the range  $0 < \Delta T_n \leq 1$  and let the subscripts  $n-1$  and  $n$  denote quantities evaluated at the pseudo times  $T_{n-1}$  and  $T_n = T_{n-1} + \Delta T_n$ . With the explicit Euler method, the values for  $\boldsymbol{\sigma}$  and  $\mathcal{H}$  at the end of a pseudo time step  $\Delta T_n$  are found from:

$$\begin{aligned} \boldsymbol{\sigma}_n &= \boldsymbol{\sigma}_{n-1} + \Delta\boldsymbol{\sigma}_1, \\ \mathcal{H}_n &= \mathcal{H}_{n-1} + \Delta\mathcal{H}_1, \end{aligned} \quad (21)$$

where:

$$\begin{aligned} \Delta\boldsymbol{\sigma}_1 &= \mathbf{D}_{ep}(\boldsymbol{\sigma}_{n-1}, \mathcal{H}_{n-1}) \Delta\boldsymbol{\epsilon}_n, \\ \Delta\mathcal{H}_1 &= \Delta\lambda(\boldsymbol{\sigma}_{n-1}, \mathcal{H}_{n-1}, \Delta\boldsymbol{\epsilon}_n) B(\boldsymbol{\sigma}_{n-1}), \end{aligned} \quad (22)$$

and:

$$\Delta\boldsymbol{\epsilon}_n = \Delta T_n \Delta\boldsymbol{\epsilon}.$$

A more accurate estimate of the stresses and hardening parameter at the end of the interval  $\Delta T_n$  can be found using the modified Euler procedure. This gives:

$$\begin{aligned}\hat{\boldsymbol{\sigma}}_n &= \boldsymbol{\sigma}_{n-1} + \frac{1}{2}(\Delta\boldsymbol{\sigma}_1 + \Delta\boldsymbol{\sigma}_2), \\ \hat{\mathcal{H}}_n &= \mathcal{H}_{n-1} + \frac{1}{2}(\Delta\mathcal{H}_1 + \Delta\mathcal{H}_2),\end{aligned}\quad (23)$$

where  $\Delta\boldsymbol{\sigma}_1$  and  $\Delta\mathcal{H}_1$  are computed from the Euler scheme and:

$$\begin{aligned}\Delta\boldsymbol{\sigma}_2 &= \mathbf{D}_{\text{ep}}(\boldsymbol{\sigma}_{n-1} + \Delta\boldsymbol{\sigma}_1, \mathcal{H}_{n-1} + \Delta\mathcal{H}_1)\Delta\boldsymbol{\epsilon}_n, \\ \Delta\mathcal{H}_2 &= \Delta\lambda(\boldsymbol{\sigma}_{n-1} + \Delta\boldsymbol{\sigma}_1, \mathcal{H}_{n-1} + \Delta\mathcal{H}_1, \Delta\boldsymbol{\epsilon}_n)B(\boldsymbol{\sigma}_{n-1} + \Delta\boldsymbol{\sigma}_1).\end{aligned}$$

Since the local error in the Euler and modified Euler solutions is  $O(\Delta T^2)$  and  $O(\Delta T^3)$  respectively, the error in  $\boldsymbol{\sigma}_n$  and  $\mathcal{H}_n$  can be estimated from:

$$\begin{Bmatrix} \hat{\boldsymbol{\sigma}}_n \\ \hat{\mathcal{H}}_n \end{Bmatrix} - \begin{Bmatrix} \boldsymbol{\sigma}_n \\ \mathcal{H}_n \end{Bmatrix} = \begin{Bmatrix} \frac{1}{2}(\Delta\boldsymbol{\sigma}_2 - \Delta\boldsymbol{\sigma}_1) \\ \frac{1}{2}(\Delta\mathcal{H}_2 - \Delta\mathcal{H}_1) \end{Bmatrix}.$$

Using any convenient norm, this quantity can be used to compute the relative error measure:

$$R_n = \frac{1}{2} \max \left\{ \frac{\|\Delta\boldsymbol{\sigma}_2 - \Delta\boldsymbol{\sigma}_1\|}{\|\hat{\boldsymbol{\sigma}}_n\|}, \frac{|\Delta\mathcal{H}_2 - \Delta\mathcal{H}_1|}{\hat{\mathcal{H}}_n} \right\}, \quad (24)$$

where the stresses are treated separately from the hardening parameter to allow for differences of scale. Once this error measure has been computed, the current strain subincrement is accepted if  $R_n$  is not greater than some prescribed tolerance,  $STOL$ , and rejected otherwise. Regardless of whether the subincrement is accepted or rejected, the next pseudo time step is found from the relation:

$$\Delta T_{n+1} = q\Delta T_n, \quad (25)$$

where  $q$  is chosen so that  $R_{n+1}$  satisfies the constraint:

$$R_{n+1} \leq STOL. \quad (26)$$

Since the local truncation error in the Euler method is  $O(\Delta T^2)$ , it follows from equation (25) that:

$$R_{n+1} \approx q^2 R_n,$$

which, combined with the constraint (26), gives:

$$q \leq \sqrt{STOL/R_n}.$$

This procedure for determining  $q$  is based on the expression for the dominant error term. Because this approximation may become inaccurate for strongly non-linear behaviour, it is wise to choose  $q$  conservatively to minimise the number of

rejected strain subincrements. Numerical experiments on a wide variety of plasticity problems suggest that a suitable strategy for computing  $q$  is to set:

$$q = 0.9\sqrt{STOL/R_n}, \quad (27)$$

and also constrain it to lie within the limits:

$$0.1 \leq q \leq 1.1, \quad (28)$$

so that:

$$0.1\Delta T_{n-1} \leq \Delta T_n \leq 1.1\Delta T_{n-1}.$$

The coefficient of 0.9 acts merely as a safety factor, since it aims to prevent the step control mechanism from choosing strain subincrements which just fail to meet the local error tolerance. Restricting the growth of consecutive strain subincrements to 10 percent also has this effect. Numerical experiments indicate that increasing the maximum growth factor for consecutive subincrements to 100 percent has little influence on the performance of the algorithm. Relaxing these constraints leads to larger subincrement sizes and fewer strain subincrements overall, but this saving is counteracted by the increased number of failed subincrements. Two final controls, of lesser importance than the above refinements, impose a minimum absolute step size,  $\Delta T_{\min}$ , and prohibit the step size from growing immediately after a failed subincrement. The first condition is added merely for robustness, and is usually not invoked unless the constitutive law contains gradient singularities. The second condition ensures there are at least two strain subincrements of the same size following a failure, and is useful for cases where the stress-strain path has sharp changes in curvature.

The integration scheme is started by applying equations (21) and (22) with the known strains  $\Delta \boldsymbol{\epsilon}$ , the initial stresses  $\boldsymbol{\sigma}_0$ , the initial hardening parameter  $\mathcal{H}_0$ , and an initial pseudo time step  $\Delta T_1$ . To allow for the case where no substeps are needed, and thus minimise the total number of strain subincrements for each Gauss point,  $\Delta T_1$  is typically set to unity. If the relative error in the resulting solution, as defined by equation (24), is not greater than the specified tolerance  $STOL$ , then the current subincrement is accepted and the stresses and hardening parameter are updated using either equation (21) or equation (23). In practice, it is best to employ the higher order update rather than the lower order update, since this is the most accurate of the two and has already been calculated. The extra accuracy of the higher order update also compensates for the fact that equation (24) is only a local and not a global error indicator. After a successful subincrement, the new stresses and hardening parameter are corrected back to the yield surface using the procedure described in section 3.3. If  $R_n > STOL$ , so that the specified error tolerance is not met, then the solution is rejected and a smaller step size is computed using equations (27) and (28). The stage is then repeated and, if necessary, the step size is reduced further until a successful subincrement size is obtained. Irrespective of whether the current subincrement is accepted or not, the size of the next strain

subincrement is found using equations (27) and (28). In successive steps, the subincrements may become larger, smaller, or stay the same, depending on the error that is calculated from equation (24). The end of the integration procedure is reached when the entire increment of strain is applied so that:

$$\sum \Delta T = T = 1.$$

The complete explicit modified Euler algorithm for critical state models, which includes all of the refinements described in the previous sections, may be summarised as follows.

*Explicit modified Euler algorithm with substepping for critical state models:*

- (1) Enter with initial stresses  $\boldsymbol{\sigma}_0$ , initial hardening parameter  $\mathcal{H}_0$ , the strain increment for the current step  $\Delta\boldsymbol{\epsilon}$  and the error tolerance for the stresses  $STOL$ .
- (2) Compute the stress increment  $\Delta\bar{\boldsymbol{\sigma}}_e$  and the trial elastic stress state  $\bar{\boldsymbol{\sigma}}_e$  according to:
 
$$\Delta\bar{\boldsymbol{\sigma}}_e = \bar{\mathbf{D}}_e(\boldsymbol{\sigma}_0, \Delta\varepsilon_v)\Delta\boldsymbol{\epsilon},$$

$$\bar{\boldsymbol{\sigma}}_e = \boldsymbol{\sigma}_0 + \Delta\bar{\boldsymbol{\sigma}}_e.$$
 If  $f(\bar{\boldsymbol{\sigma}}_e, \mathcal{H}_0) \leq FTOL$  then the stress increment is purely elastic, so set  $\boldsymbol{\sigma}_0 = \bar{\boldsymbol{\sigma}}_e$  and  $\mathcal{H}_1 = \mathcal{H}_0$  and go to step 16.
- (3) If  $f(\boldsymbol{\sigma}_0, \mathcal{H}_0) < -FTOL$  and  $f(\bar{\boldsymbol{\sigma}}_e, \mathcal{H}_0) > FTOL$  then the stress point undergoes a transition from elastic to plastic behaviour. Compute the portion of  $\Delta\boldsymbol{\epsilon}$  that corresponds to purely elastic deformation,  $\alpha$ , using the Pegasus intersection scheme of section 3.1 and go to step 5.
- (4) If  $|f(\boldsymbol{\sigma}_0, \mathcal{H}_0)| \leq FTOL$  and  $f(\bar{\boldsymbol{\sigma}}_e, \mathcal{H}_0) > FTOL$  then:
 Check for a elastoplastic unloading by computing:

$$\cos \theta = \frac{\mathbf{a}^T \Delta\boldsymbol{\sigma}_e}{\|\mathbf{a}\|_2 \|\Delta\boldsymbol{\sigma}_e\|_2},$$

where  $\mathbf{a}$  is evaluated at  $\boldsymbol{\sigma}_0$  and  $\Delta\boldsymbol{\sigma}_e$  is found using the tangential elastic stiffness matrix according to:

$$\Delta\boldsymbol{\sigma}_e = \mathbf{D}_e(\boldsymbol{\sigma}_0)\Delta\boldsymbol{\epsilon}.$$

If  $\cos \theta \geq -LTOL$  then:

The stress increment is purely plastic, so set  $\alpha = 0$ .

else:

Elastic unloading followed by plastic flow occurs. Compute the portion of  $\Delta\boldsymbol{\epsilon}$  that corresponds to purely elastic deformation,  $\alpha$ , using the Pegasus intersection scheme for elastoplastic unloading described in section 3.2.

else:

The stress state is illegal as it lies outside the yield surface.

- (5) Update the stresses at the onset of plastic yielding as  $\boldsymbol{\sigma}_0 \leftarrow \boldsymbol{\sigma}_0 + \alpha \bar{\mathbf{D}}_e(\boldsymbol{\sigma}_0, \alpha \Delta \varepsilon_v) \Delta \boldsymbol{\varepsilon}$ . Then compute the portion of  $\Delta \boldsymbol{\varepsilon}$  that corresponds to plastic deformation according to  $\Delta \boldsymbol{\varepsilon} \leftarrow (1 - \alpha) \Delta \boldsymbol{\varepsilon}$ .
- (6) Set  $T = 0$  and  $\Delta T = 1$ .
- (7) While  $T < 1$ , perform steps 8-15.
- (8) Compute  $\Delta \boldsymbol{\sigma}_i$  and  $\Delta \mathcal{H}_i$  for  $i = 1$  to 2 using:

$$\begin{aligned} \Delta \boldsymbol{\sigma}_{ei} &= \mathbf{D}_{ei} \Delta T \Delta \boldsymbol{\varepsilon}, \\ \Delta \boldsymbol{\sigma}_i &= \Delta \boldsymbol{\sigma}_{ei} = -\Delta \lambda_i \mathbf{D}_{ei} \mathbf{B}_i, \\ \Delta \mathcal{H}_i &= \Delta \lambda_i B_i, \end{aligned}$$

where:

$$\Delta \lambda_i = \max \left\{ \frac{\mathbf{a}_i^T \Delta \boldsymbol{\sigma}_{ei}}{A_i + \mathbf{a}_i^T \mathbf{D}_{ei} \mathbf{b}_i}, 0 \right\},$$

$$B_i = -\frac{A_i}{\partial f / \partial \mathcal{H}} = \frac{vp'_0}{\lambda - k} \left( \frac{\partial g}{\partial p'} \right)_i,$$

$$A_i = -(\partial f / \partial \mathcal{H}) B_i,$$

$$\mathbf{a}_i = \left( \frac{\partial f}{\partial \boldsymbol{\sigma}} \right)_i,$$

$$\mathbf{b}_i = \left( \frac{\partial g}{\partial \boldsymbol{\sigma}} \right)_i,$$

$$\mathbf{D}_{ei} = \mathbf{D}_e(\boldsymbol{\sigma}_i),$$

are evaluated at  $(\tilde{\boldsymbol{\sigma}}_i, \tilde{\mathcal{H}}_i)$ , and:

$$\begin{aligned} \tilde{\boldsymbol{\sigma}}_i &= \boldsymbol{\sigma}_T & \tilde{\mathcal{H}}_i &= \mathcal{H}_T \\ \tilde{\boldsymbol{\sigma}}_2 &= \boldsymbol{\sigma}_T + \Delta \boldsymbol{\sigma}_1 & \tilde{\mathcal{H}}_2 &= \mathcal{H}_T + \Delta \mathcal{H}_1 \end{aligned}$$

- (9) Compute the new stresses and hardening parameter and hold them in temporary storage according to:
- $$\begin{aligned} \tilde{\boldsymbol{\sigma}}_{T+\Delta T} &= \boldsymbol{\sigma}_T + \frac{1}{2} \Delta \boldsymbol{\sigma}_1 + \Delta \boldsymbol{\sigma}_2, \\ \tilde{\mathcal{H}}_{T+\Delta T} &= \mathcal{H}_T + \frac{1}{2} (\Delta \mathcal{H}_1 + \Delta \mathcal{H}_2). \end{aligned}$$
- (10) Determine the relative error for the current substep from:

$$R_{T+\Delta T} = \max \left\{ \frac{\|\Delta \boldsymbol{\sigma}_2 - \Delta \boldsymbol{\sigma}_1\|}{2\|\tilde{\boldsymbol{\sigma}}_{T+\Delta T}\|}, \frac{|\Delta \mathcal{H}_2 - \Delta \mathcal{H}_1|}{2\tilde{\mathcal{H}}_{T+\Delta T}}, EPS \right\},$$

where *EPS* is a machine constant indicating the smallest relative error that can be calculated.

- (11) If  $R_{T+\Delta T} > STOL$  the substep has failed and a smaller pseudo time step needs to be found by extrapolation. First compute:

$$q = \max\left\{0.9\sqrt{STOL/R_{T+\Delta T}}, 0.1\right\},$$

and then set:

$$\Delta T \leftarrow \max\{q\Delta T, \Delta T_{\min}\},$$

before returning to step 8.

- (12) The substep is successful, so update the stresses and the hardening parameter according to:

$$\boldsymbol{\sigma}_{T+\Delta T} = \tilde{\boldsymbol{\sigma}}_{T+\Delta T},$$

$$\mathcal{H}_{T+\Delta T} = \mathcal{H}_{T+\Delta T}.$$

- (13) If  $|f(\boldsymbol{\sigma}_{T+\Delta T}, \mathcal{H}_{T+\Delta T})| > FTOL$ , then correct  $\boldsymbol{\sigma}_{T+\Delta T}$  and  $\mathcal{H}_{T+\Delta T}$  back to the yield surface using the algorithm of section 3.3

- (14) Extrapolate to obtain the size of the next substep by computing:

$$q = \min\left\{0.9\sqrt{STOL/R_{T+\Delta T}}, 1.1\right\}.$$

If the previous step failed, limit the step size growth further by enforcing:

$$q = \min\{q, 1\}.$$

Compute new step size and update pseudo time according to:

$$\Delta T \leftarrow q\Delta T,$$

$$\Delta T \leftarrow T + \Delta T.$$

- (15) Ensure the next step size is not smaller than the minimum step size and check that integration does not proceed beyond  $T = 1$  by setting:

$$\Delta T \leftarrow \max\{\Delta T, \Delta T_{\min}\},$$

and then:

$$\Delta T \leftarrow \min\{\Delta T, 1 - T\}.$$

- (16) Exit with stresses  $\boldsymbol{\sigma}_1$  and hardening parameter  $\mathcal{H}_1$  at end of increment with  $T = 1$ .

For the case of conventional elastoplastic models with a constant elastic stress-strain matrix, steps 2-8 in the algorithm above can be simplified as follows.

*Explicit modified Euler algorithm with substepping for conventional elastoplastic models:*

- (2) Compute the stress increment  $\Delta\boldsymbol{\sigma}_e$  and the trial elastic stress state  $\boldsymbol{\sigma}_e$  according to:

$$\Delta\boldsymbol{\sigma}_e = \mathbf{D}_e\Delta\boldsymbol{\varepsilon},$$

$$\boldsymbol{\sigma}_e = \boldsymbol{\sigma}_0 + \Delta\boldsymbol{\sigma}_e.$$

If  $f(\boldsymbol{\sigma}_e, \mathcal{H}_0) \leq FTOL$  then the stress increment is purely elastic, so set  $\boldsymbol{\sigma}_1 = \boldsymbol{\sigma}_e$  and  $\mathcal{H}_1 = \mathcal{H}_0$  and go to step 16.

- (3) If  $f(\boldsymbol{\sigma}_0, \mathcal{H}_0) < -FTOL$  and  $f(\boldsymbol{\sigma}_e, \mathcal{H}_0) > FTOL$  then the stress point undergoes a transition from elastic to plastic behaviour. Compute the

portion of  $\Delta \boldsymbol{\epsilon}$  that corresponds to purely elastic deformation,  $\alpha$ , using the Pegasus intersection scheme of section 3.1 and go to step 5.

- (4) If  $f(\boldsymbol{\sigma}_0, \mathcal{H}_0) \leq FTOL$  and  $f(\boldsymbol{\sigma}_e, \mathcal{H}_0) > FTOL$  then:  
Check for a elastoplastic unloading by computing:

$$\cos \theta = \frac{\mathbf{a}^T \Delta \boldsymbol{\sigma}_e}{\|\mathbf{a}\|_2 \|\Delta \boldsymbol{\sigma}_e\|_2},$$

where  $\mathbf{a}$  is evaluated at  $\boldsymbol{\sigma}_0$ .

If  $\cos \theta \geq -LTOL$  then:

The stress increment is purely plastic, so set  $\alpha = 0$ .

else:

Elastic unloading followed by plastic flow occurs. Compute the portion of  $\Delta \boldsymbol{\epsilon}$  that corresponds to purely elastic deformation,  $\alpha$ , using the Pegasus intersection scheme for elastoplastic unloading described in section 3.2.

else:

The stress state is illegal as it lies outside the yield surface.

- (5) Update the stresses at the onset of plastic yielding as  $\boldsymbol{\sigma}_0 \leftarrow \boldsymbol{\sigma}_0 + \alpha \Delta \boldsymbol{\sigma}_e$ . Then compute the portion of  $\Delta \boldsymbol{\sigma}_e$  that corresponds to plastic deformation according to  $\Delta \boldsymbol{\sigma}_e \leftarrow (1 - \alpha) \Delta \boldsymbol{\sigma}_e$ .
- (6) Set  $T = 0$  and  $\Delta T = 1$ .
- (7) While  $T < 1$ , perform steps 8-15.
- (8) Compute  $\Delta \boldsymbol{\sigma}_i$  and  $\Delta \mathcal{H}_i$  for  $i = 1$  to 2 using:  

$$\Delta \boldsymbol{\sigma}_i = \Delta T \Delta \boldsymbol{\sigma}_e - \Delta \lambda_i \mathbf{D}_e \mathbf{b}_i,$$

$$\Delta \mathcal{H}_i = \Delta \lambda_i B_i,$$
where:

$$\Delta \lambda_i = \max \left\{ \frac{\Delta T \mathbf{a}_i^T \Delta \boldsymbol{\sigma}_e}{A_i + \mathbf{a}_i^T \mathbf{D}_e \mathbf{b}_i}, 0 \right\},$$

$$B_i = - \frac{A_i}{\partial f / \partial \mathcal{H}} = \begin{cases} \sqrt{\frac{2}{3}} \mathbf{b}_i^T \mathbf{M} \mathbf{b}_i & \text{strain hardening} \\ \boldsymbol{\sigma}_i^T \mathbf{b}_i & \text{work hardening} \end{cases}$$

$$A_i = - - (\partial f / \partial \mathcal{H}) B_i,$$

$$\mathbf{a}_i = \left( \frac{\partial f}{\partial \boldsymbol{\sigma}} \right)_i,$$

$$\mathbf{b}_i = \left( \frac{\partial g}{\partial \boldsymbol{\sigma}} \right)_i,$$

are evaluated at  $(\tilde{\boldsymbol{\sigma}}_i, \tilde{\mathcal{H}}_i)$ , and

$$\begin{aligned}\tilde{\sigma}_1 &= \sigma_T & \tilde{\mathcal{H}}_1 &= \mathcal{H}_T \\ \tilde{\sigma}_2 &= \sigma_T + \Delta\sigma_1 & \tilde{\mathcal{H}}_2 &= \mathcal{H}_T + \Delta\mathcal{H}_1\end{aligned}$$

For double precision arithmetic on a 32-bit machine, appropriate values for the tolerances in steps 4 and 10 are  $LTOL \approx 10^{-6}$  and  $EPS 10^{-16}$ .

The above schemes incorporate several key improvements to the original integration procedure of Sloan (1987). These include the generalisation to cover critical state soil models, the Pegasus method for computing the elastic-plastic transition point on the yield surface, the new scheme for dealing with elastoplastic unloading, and the consistent yield surface correction procedure. Apart from these algorithmic changes, a number of tuning adjustments have also been made in light of extensive numerical experiments. The safety factor coefficient on the subincrement size, originally 0.8, has been increased to 0.9 to give better control of the integration process. To minimise the number of rejected substeps, the maximum growth in size between successive subincrements has been reduced from 100 percent to 10 percent and no growth in the step size is now permitted for the two subincrements that immediately follow a failed step. In the event that a discontinuous yield surface is employed, a minimum step size has also been introduced to force the integration of the constitutive equations. Typical values for the minimum substep size  $\Delta T_{\min}$  are of the order of  $10^{-4}$ , which implies that a maximum of 10,000 substeps may be used at a Gauss point during a load step or iteration.

### 3.5 Single step modified Euler scheme

A single step modified Euler scheme can be derived from the previous algorithm merely by setting the integration tolerance  $STOL$  to a large value. Results from this type of method will be discussed later to indicate the accuracy of explicit integration schemes that do not employ subincrementation.

### 3.6 Runge-Kutta-Dormand-Prince scheme with substepping

The explicit Runge-Kutta-Dormand-Prince scheme is similar to the modified Euler scheme described above except that a pair of fourth and fifth order integration formulae are used to perform the integration (Sloan and Booker, 1992). With this high order algorithm, the stresses and hardening parameter at the end of each subincrement are usually very accurate and seldom need to be corrected back to the yield surface to satisfy the yield tolerance. The Runge-Kutta-Dormand-Prince scheme is especially useful for checking the accuracy of lower order methods, as it can be used with a stringent stress tolerance of  $STOL = 10^{-9}$  or smaller.

When applied to equations (19) and (20) with a pseudo time step  $\Delta T_n$ , the fourth and fifth order accurate solutions for the stresses and hardening parameters are given by:

$$\begin{aligned}\boldsymbol{\sigma}_n &= \boldsymbol{\sigma}_{n-1} + \frac{31}{540} \Delta \boldsymbol{\sigma}_1 + \frac{190}{297} \Delta \boldsymbol{\sigma}_3 - \frac{145}{108} \Delta \boldsymbol{\sigma}_4 + \frac{351}{220} \Delta \boldsymbol{\sigma}_5 + \frac{1}{20} \Delta \boldsymbol{\sigma}_6, \\ \mathcal{H}_n &= \mathcal{H}_{n-1} + \frac{31}{540} \Delta \mathcal{H}_1 + \frac{190}{297} \Delta \mathcal{H}_3 - \frac{145}{108} \Delta \mathcal{H}_4 + \frac{351}{220} \Delta \mathcal{H}_5 + \frac{1}{20} \Delta \mathcal{H}_6,\end{aligned}\quad (29)$$

and:

144

---


$$\begin{aligned}\hat{\boldsymbol{\sigma}}_n &= \boldsymbol{\sigma}_{n-1} + \frac{19}{216} \Delta \boldsymbol{\sigma}_1 + \frac{1,000}{2,079} \Delta \boldsymbol{\sigma}_3 - \frac{125}{216} \Delta \boldsymbol{\sigma}_4 + \frac{81}{88} \Delta \boldsymbol{\sigma}_5 + \frac{5}{56} \Delta \boldsymbol{\sigma}_6, \\ \hat{\mathcal{H}}_n &= \mathcal{H}_{n-1} + \frac{19}{216} \Delta \mathcal{H}_1 + \frac{1,000}{2,079} \Delta \mathcal{H}_3 - \frac{125}{216} \Delta \mathcal{H}_4 - \frac{81}{88} \Delta \mathcal{H}_5 + \frac{5}{56} \Delta \mathcal{H}_6,\end{aligned}\quad (30)$$

where:

$$\left. \begin{aligned}\Delta \boldsymbol{\sigma}_i &= \mathbf{D}_{\text{ep}}(\hat{\boldsymbol{\sigma}}_i, \hat{\mathcal{H}}_i) \Delta \boldsymbol{\varepsilon}_n \\ \Delta \mathcal{H}_i &= \Delta \lambda(\hat{\boldsymbol{\sigma}}_i, \hat{\mathcal{H}}_i, \Delta \boldsymbol{\varepsilon}_n) B(\boldsymbol{\sigma}_i) \\ \Delta \boldsymbol{\varepsilon}_n &= \Delta T_n \Delta \boldsymbol{\varepsilon}\end{aligned}\right\} \text{ for } i = 1, 2, \dots, 6,$$

and:

$$\begin{aligned}\tilde{\boldsymbol{\sigma}}_1 &= \boldsymbol{\sigma}_{n-1}, \\ \tilde{\mathcal{H}}_1 &= \mathcal{H}_{n-1},\end{aligned}\quad (31)$$

$$\begin{aligned}\tilde{\boldsymbol{\sigma}}_2 &= \boldsymbol{\sigma}_{n-1} + \frac{1}{5} \Delta \boldsymbol{\sigma}_1, \\ \tilde{\mathcal{H}}_2 &= \mathcal{H}_{n-1} + \frac{1}{5} \Delta \mathcal{H}_1,\end{aligned}\quad (32)$$

$$\begin{aligned}\tilde{\boldsymbol{\sigma}}_3 &= \boldsymbol{\sigma}_{n-1} + \frac{3}{40} \Delta \boldsymbol{\sigma}_1 + \frac{9}{40} \Delta \boldsymbol{\sigma}_2, \\ \tilde{\mathcal{H}}_3 &= \mathcal{H}_{n-1} + \frac{3}{40} \Delta \mathcal{H}_1 + \frac{9}{40} \Delta \mathcal{H}_2,\end{aligned}\quad (33)$$

$$\begin{aligned}\tilde{\boldsymbol{\sigma}}_4 &= \boldsymbol{\sigma}_{n-1} + \frac{3}{10} \Delta \boldsymbol{\sigma}_1 - \frac{9}{10} \Delta \boldsymbol{\sigma}_2 + \frac{6}{5} \Delta \boldsymbol{\sigma}_3, \\ \tilde{\mathcal{H}}_4 &= \mathcal{H}_{n-1} + \frac{3}{10} \Delta \mathcal{H}_1 - \frac{9}{10} \Delta \mathcal{H}_2 + \frac{6}{5} \Delta \mathcal{H}_3,\end{aligned}\quad (34)$$

$$\begin{aligned}\tilde{\boldsymbol{\sigma}}_5 &= \boldsymbol{\sigma}_{n-1} + \frac{226}{729} \Delta \boldsymbol{\sigma}_1 - \frac{25}{27} \Delta \boldsymbol{\sigma}_2 + \frac{880}{729} \Delta \boldsymbol{\sigma}_3 + \frac{55}{729} \Delta \boldsymbol{\sigma}_4, \\ \tilde{\mathcal{H}}_5 &= \mathcal{H}_{n-1} + \frac{226}{729} \Delta \mathcal{H}_1 - \frac{25}{27} \Delta \mathcal{H}_2 + \frac{880}{729} \Delta \mathcal{H}_3 + \frac{55}{729} \Delta \mathcal{H}_4,\end{aligned}\quad (35)$$

$$\begin{aligned}\tilde{\sigma}_6 &= \sigma_{n-1} - \frac{181}{270} \Delta \sigma_1 + \frac{5}{2} \Delta \sigma_2 - \frac{226}{297} \Delta \sigma_3 - \frac{91}{27} \Delta \sigma_4 + \frac{189}{55} \Delta \sigma_5, \\ \tilde{\mathcal{H}}_6 &= \mathcal{H}_{n-1} - \frac{181}{270} \Delta \mathcal{H}_1 + \frac{5}{2} \Delta \mathcal{H}_2 - \frac{226}{297} \Delta \mathcal{H}_3 - \frac{91}{27} \Delta \mathcal{H}_4 + \frac{189}{55} \Delta \mathcal{H}_5.\end{aligned}\quad (36)$$

Subtracting equations (29) from equations (30) gives a fifth order accurate estimate of the local truncation error according to:

$$\left\{ \begin{array}{c} \hat{\sigma}_n \\ \hat{\mathcal{H}}_n \end{array} \right\} - \left\{ \begin{array}{c} \sigma_n \\ \mathcal{H}_n \end{array} \right\} = \left\{ \begin{array}{c} \frac{11}{360} \Delta \sigma_1 - \frac{10}{63} \Delta \sigma_3 + \frac{55}{72} \Delta \sigma_4 - \frac{27}{40} \Delta \sigma_5 + \frac{11}{280} \Delta \sigma_6 \\ \frac{11}{360} \Delta \mathcal{H}_1 - \frac{10}{63} \Delta \mathcal{H}_3 + \frac{55}{72} \Delta \mathcal{H}_4 - \frac{27}{40} \Delta \mathcal{H}_5 + \frac{11}{280} \Delta \mathcal{H}_6 \end{array} \right\}$$

The theory for implementing the explicit Dormand-Prince formulae is identical to that for the modified Euler scheme. Steps 8-11 and 14 of the algorithm of section 3.4 need to be changed as follows:

- (8) The variable  $i$  ranges from 1 to 6 and  $\tilde{\sigma}_i$  and  $\tilde{\mathcal{H}}_i$  are given by equations (31)-(36).
- (9) Compute the new stresses and hardening parameter and hold them in temporary storage according to:

$$\begin{aligned}\tilde{\sigma}_{T+\Delta T} &= \sigma_T + \frac{19}{216} \Delta \sigma_1 + \frac{1,000}{2,079} \Delta \sigma_3 - \frac{125}{216} \Delta \sigma_4 + \frac{81}{88} \Delta \sigma_5 + \frac{5}{56} \Delta \sigma_6, \\ \tilde{\mathcal{H}}_{T+\Delta T} &= \mathcal{H}_T + \frac{19}{216} \Delta \mathcal{H}_1 + \frac{1,000}{2,079} \Delta \mathcal{H}_3 - \frac{125}{216} \Delta \mathcal{H}_4 - \frac{81}{88} \Delta \mathcal{H}_5 + \frac{5}{56} \Delta \mathcal{H}_6.\end{aligned}$$

- (10) Determine the relative error for the current substep from:

$$R_{T+\Delta T} = \max \left\{ \frac{\|E_{T+\Delta T}^\sigma\|}{\|\hat{\sigma}_{T+\Delta T}\|}, \frac{|E_{T+\Delta T}^{\mathcal{H}}|}{\tilde{\mathcal{H}}_{T+\Delta T}}, EPS \right\},$$

where:

$$\begin{aligned}E_{T+\Delta T}^\sigma &= \frac{11}{360} \Delta \sigma_1 - \frac{10}{63} \Delta \sigma_3 + \frac{55}{72} \Delta \sigma_4 - \frac{27}{40} \Delta \sigma_5 + \frac{11}{280} \Delta \sigma_6, \\ E_{T+\Delta T}^{\mathcal{H}} &= \frac{11}{360} \Delta \mathcal{H}_1 - \frac{10}{63} \Delta \mathcal{H}_3 + \frac{55}{72} \Delta \mathcal{H}_4 - \frac{27}{40} \Delta \mathcal{H}_5 + \frac{11}{280} \Delta \mathcal{H}_6,\end{aligned}$$

and  $EPS$  is a machine constant indicating the smallest relative error that can be calculated.

- (11) If  $R_{T+\Delta T} > STOL$  the substep has failed and a smaller pseudo time step needs to be found by extrapolation. First compute:

$$q = \max\{0.9(STOL/R_{T+\Delta T})^{1/5}, 0.1\},$$

and then set:

$$\Delta T \leftarrow \max\{q\Delta T, \Delta T_{\min}\}, \text{ before returning to step 8.}$$

(14) Extrapolate to obtain the size of the next substep by computing:

$$q = \min\{0.9(STOL/R_{T+\Delta T})^{1/5}, 1.1\},$$

If the previous step failed, limit the step size growth further by enforcing:

$$q = \min\{q, 1\}.$$

Compute new step size and update pseudo time according to:

$$\Delta T \leftarrow q\Delta T,$$

$$T \leftarrow T + \Delta T.$$

The extra accuracy of the Dormand-Prince scheme is obtained at the expense of additional evaluations of the constitutive relations for each subincrement. Six evaluations per subincrement are needed, as opposed to two for the modified Euler algorithm.

#### 4. Performance of integration schemes

To compare the numerical performance of the explicit integration schemes described in the previous sections, we now consider the behaviour of a smooth rigid strip footing resting on an elastoplastic soil mass. This is a good test case for assessing various integration strategies due to the singularity at the edge of the footing and the strong rotation of the principal stresses.

The soil mass is discretised using the mesh of triangular cubic strain elements shown in Figure 5. As discussed by Sloan and Randolph (1982), these elements can predict incompressible plastic flow accurately and efficiently without the need for reduced/selective integration or other numerical approximations. In the first example, undrained loading of the soil is modelled

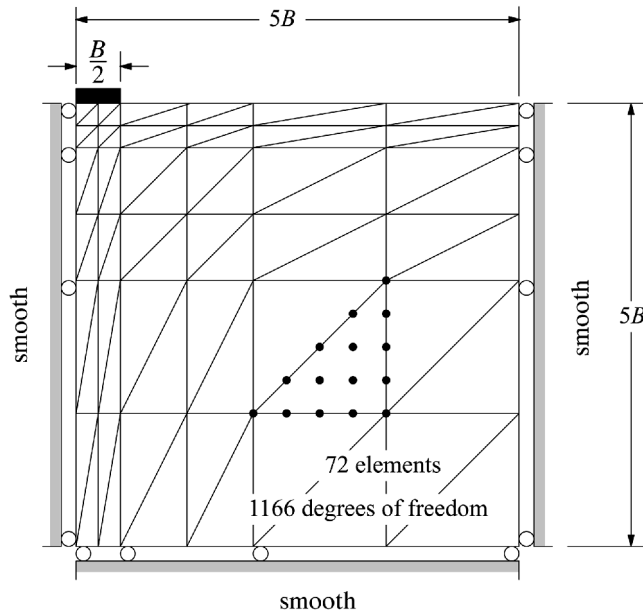


Figure 5.  
Footing mesh

using a rounded Tresca yield surface (Sloan and Booker, 1986). For the remaining cases, drained analyses are carried out for a rounded hyperbolic Mohr-Coulomb yield surface (Abbo, 1997), a modified Cam clay model, and a generalised Cam clay model.

In all analyses, a non-iterative tangent stiffness method is used to solve the governing stiffness equations and the footing is loaded by prescribed displacement increments of equal size. The size of these increments is set so that the final displacement induces a state of collapse in the soil mass. At the end of each displacement increment, the unbalanced nodal forces are calculated and added to the next increment to minimise the drift from equilibrium. This type of scheme corresponds to a forward Euler integration with a load correction and is simple to implement.

To assess the accuracy of each scheme, the stress integration error is estimated from the expression:

$$\sigma_{\text{error}} = \frac{\left\{ \sum_{i=1}^m [(\boldsymbol{\sigma}_{\text{ref}} - \boldsymbol{\sigma})^T (\boldsymbol{\sigma}_{\text{ref}} - \boldsymbol{\sigma})]_i \right\}^{1/2}}{\left\{ \sum_{i=1}^m [(\boldsymbol{\sigma}_{\text{ref}})^T (\boldsymbol{\sigma}_{\text{ref}})]_i \right\}^{1/2}}, \quad (37)$$

where the subscript  $i$  refers to each integration point,  $m$  is the total number of integration points in the mesh,  $\boldsymbol{\sigma}$  are the stresses computed at the end of the last load increment, and  $\boldsymbol{\sigma}_{\text{ref}}$  are “reference” stresses found using the explicit Runge-Kutta-Dormand-Prince (RKDP) integration scheme with a stress tolerance of  $STOL = 10^{-9}$ . The reference stresses provide a very accurate set of stresses for a given mesh, loading sequence, and solution method and can be used to check the accuracy of various integration schemes. Indeed, for the modified Euler runs with substepping, the error computed from equation (37) may be compared directly with the stress tolerance  $STOL$  to gauge the performance of the error control mechanism. Note that a Euclidean norm is used to measure the stress error in equation (37) because this matches the norm used in the explicit subincrementation schemes, but other consistent sets of norms may also be adopted. In all runs, the stresses are restored to the yield surface using an absolute tolerance of  $FTOL = 10^{-9}$ .

For the analyses with non-hardening models, an additional check on the accuracy of the solutions can be obtained by comparing their collapse pressures against the exact results from classical plasticity theory. In these comparisons, an equivalent uniform pressure  $w$  is found by summing the reactions at the footing nodes which have prescribed vertical displacements. Because the numerical footing loads contain spatial discretisation error, we expect them to differ from the exact values, even for analyses with very small stress integration errors.

The soil properties used in the various analyses are summarised in Table I. To investigate the influence of the flow rule on the performance of the

**Table I.**  
Material properties of  
soil layers

Material property		Tresca (A)	Mohr-Coulomb (A)	Mohr-Coulomb (NA)	Modified Cam clay (A)	Generalised Cam clay (A)
Young's modulus	E	298	1,040	1,040	–	–
Soil unit weight	$\gamma$	–	–	–	6	6
Friction angle (degrees)	$\phi$	0	30	30	23	23
Dilation angle (degrees)	$\psi$	0	30	20	–	–
Poisson's ratio	$\mu$	0.49	0.3	0.3	0.375	0.375
Cohesion	c	1	1	1	–	–
Slope of NCL	$\lambda$	–	–	–	0.2	0.2
Slope of URL	k	–	–	–	0.03	0.03
Overconsolidation ratio	OCR	–	–	–	1	1
Void ratio at $p = 1$	$e_0$	–	–	–	2.1	2.1
Parameter	$\alpha$	–	–	–	–	0.85
Parameter	$\beta'$	–	–	–	1	1

integration schemes, the Mohr-Coulomb models are used in both associated and non-associated forms. All the timing results presented in this section are for a Pentium Pro 200 MHz processor with the Microsoft FORTRAN Powerstation 4.0 compiler. The CPU time recorded is for the entire finite element analysis, not just the stress integration, since this quantity is of primary interest in the design of finite element codes.

#### 4.1 Rigid strip footing on Tresca layer

The Tresca footing results shown in Table II include the total CPU time, the collapse pressure, the total successful substeps, the maximum number of successful substeps, and the stress error (37) for runs with the modified Euler scheme, the single step modified Euler scheme, and the Runge-Kutta-Dormand-Prince (RKDP) scheme. For the modified Euler algorithm, data is presented for stress error tolerances ranging from  $STOL = 10^{-1}$  to  $STOL = 10^{-4}$  so that the effect of this parameter can be investigated.

The collapse pressures for the modified Euler scheme are similar for all the specified stress tolerances and vary by less than 0.04 percent. They range from  $w/c = 5.4197$  for  $STOL = 10^{-1}$  to  $w/c = 5.4179$  for  $STOL = 10^{-4}$ , and are roughly

**Table II.**  
Rigid strip footing on  
Tresca layer (50 load  
steps)

Scheme	CPU time (s)	Collapse pressure ( $w/c$ )	Total success. substeps	Max. success. substeps	Stress error ( $\sigma_{error}$ )
Modified Euler					
$STOL = 10^{-1}$	142	5.4197	10,424	1	$0.59 \times 10^{-3}$
$STOL = 10^{-2}$	142	5.4193	10,434	2	$0.52 \times 10^{-3}$
$STOL = 10^{-3}$	143	5.4179	11,563	5	$0.64 \times 10^{-4}$
$STOL = 10^{-4}$	143	5.4179	19,737	13	$0.13 \times 10^{-4}$
Single step modified Euler	142	5.4179	10,424	1	$0.59 \times 10^{-3}$
Runge-Kutta-Dormand-Prince	145	5.4179	16,883	9	–

5 percent above Prandtl's exact result of  $w/c = 2 + \pi$ . It is reassuring to note that the collapse load obtained for  $STOL = 10^{-4}$  is identical to the collapse load obtained with the highly accurate RKDP method. The errors in the stresses computed from the explicit modified Euler scheme, as defined by equation (37), are always less than the integration tolerance  $STOL$  and thus give the required error control. Because a minimal amount of substepping is performed up to an integration tolerance of about  $10^{-3}$ , the error control appears conservative with stress errors which are rather smaller than  $STOL$ . For the single step modified Euler scheme, which has  $STOL = 1$ , the stress error is  $0.59 \times 10^{-3}$ . When  $STOL$  is tightened to  $STOL = 10^{-2}$ , the error is the same since no substepping is required. With the most stringent tolerance of  $STOL = 10^{-4}$ , a maximum of 13 substeps are needed and the stress error is reduced by more than one order of magnitude to  $0.13 \times 10^{-4}$ . If the stress error tolerance in the modified Euler scheme is tightened by a factor of ten, we expect the maximum number of substeps to increase by a factor of approximately  $\sqrt{10}$ . The observed growth in the maximum number of substeps is somewhat less than this prediction, probably due to the interaction between the stress integration process and the global solution method.

The overall CPU time required for each of the stress integration methods is remarkably similar, regardless of the error tolerance used to integrate the Tresca model. Although the RKDP method required the largest CPU time, this scheme was run with a very stringent tolerance of  $STOL = 10^{-9}$ .

#### 4.2 Rigid strip footing on associated Mohr-Coulomb layer

The results for the associated Mohr-Coulomb footing analyses, shown in Table III, give collapse loads ranging from  $w/c = 31.835$  down to  $w/c = 31.378$ , with the higher value being for  $STOL = 10^{-1}$  and the lower value being for  $STOL = 10^{-4}$ . These predictions are, respectively, 5.6 percent and 4.1 percent above the exact Prandtl collapse load of  $w/c = 30.140$ . Overall, the results behave as expected, with the accuracy of the collapse loads improving as the stress tolerance is tightened. As in the Tresca case, the modified Euler collapse load for  $STOL = 10^{-4}$  is the same as the collapse load for the RKDP method. The single step modified Euler method, not surprisingly, gives the least accurate collapse load.

Scheme	CPU time (s)	Collapse pressure ( $w/c$ )	Total success. substeps	Max. success. substeps	Stress error ( $\sigma_{\text{error}}$ )
Modified Euler					
$STOL = 10^{-1}$	147	31.835	19,591	25	$0.39 \times 10^{-1}$
$STOL = 10^{-2}$	148	31.410	21,995	100	$0.10 \times 10^{-1}$
$STOL = 10^{-3}$	149	31.379	29,329	283	$0.12 \times 10^{-2}$
$STOL = 10^{-4}$	150	31.378	57,065	291	$0.13 \times 10^{-3}$
Single step modified Euler	146	32.413	18,769	1	$0.67 \times 10^{-1}$
Runge-Kutta-Dormand-Prince	157	31.378	48,937	168	—

**Table III.**  
Rigid strip footing on associated Mohr-Coulomb layer (50 load steps)

The observed stress errors for the explicit modified Euler scheme are always close to the specified stress tolerance  $STOL$ . Indeed, these errors are generally within an order of magnitude of the required levels and thus display a “tolerance proportionality” which is sufficient for controlling the stress integration error. For example, the most accurate modified Euler integration with  $STOL = 10^{-4}$  gives a stress error of  $1.3 \times 10^{-4}$ , while analysis with  $STOL = 10^{-1}$  gives an error of  $0.39 \times 10^{-1}$ . Compared with the corresponding results for the Tresca soil model, the Mohr-Coulomb model typically requires more than twice the total number of substeps to achieve the same level of accuracy. This reflects the increased non-linearity of the Mohr-Coulomb relations which is caused by their dependence on mean normal stress.

The CPU times for this example again suggest that the performance of the modified Euler scheme is not particularly sensitive to the  $STOL$  values considered. These conclusions echo those for the Tresca criterion.

#### 4.3 Rigid strip footing on non-associated Mohr-Coulomb layer

The non-associated Mohr-Coulomb footing results, shown in Table IV, indicate that these analyses require roughly twice as much CPU time as their associated flow rule counterparts. This is largely due to the extra cost of solving an unsymmetric system of stiffness equations, and is not attributable to the stress integration. Although the exact collapse load for this case is unknown, the numerical results suggest it is probably very close to the associated flow rule value of  $w/c = 30.140$ .

Apart from the larger CPU times, the data in Table IV display similar trends to those for the example with an associated flow rule described previously (Table III). Indeed, many of the same observations and conclusions apply. As the observed stress errors for the modified Euler scheme are all within an order of magnitude of the specified tolerances  $STOL$ , this suggests the explicit error control also works well for a non-associated Mohr-Coulomb material.

#### 4.4 Rigid strip footing on critical state soil layers

As critical state models do not have any strength if the effective mean normal stress is zero or tensile, they require a compressive initial stress state to be

Scheme	CPU time (s)	Collapse pressure ( $w/c$ )	Total success. substeps	Max. success. substeps	Stress error ( $\sigma_{error}$ )
Modified Euler					
$STOL = 10^{-1}$	293	30.825	16,858	4	$0.78 \times 10^{-2}$
$STOL = 10^{-2}$	293	30.839	17,103	8	$0.12 \times 10^{-2}$
$STOL = 10^{-3}$	294	30.836	20,207	17	$0.91 \times 10^{-3}$
$STOL = 10^{-4}$	296	30.833	38,523	48	$0.29 \times 10^{-4}$
Single step modified Euler	293	31.045	16,690	1	$0.31 \times 10^{-1}$
Runge-Kutta-Dormand-Prince	299	30.833	30,328	74	–

**Table IV.**  
Rigid strip footing on non-associated Mohr-Coulomb layer (50 load steps)

established in the soil layer. For the examples considered here, a hydrostatic initial stress state is generated elastically by gradually applying a gravity load (due to the soil buoyant unit weight) over 50 equal sized increments. During this stage, we assume the layer is non-linear elastic with a large preconsolidation pressure  $p'_0$  to prevent plastic yielding. Once the initial stresses are established, the correct initial preconsolidation pressure for each Gauss point is found using the formula  $p'_0 = \text{OCR} \times (p'_{\text{in}})_0$ , where OCR denotes a known overconsolidation ratio (Table I) and  $(p'_{\text{in}})_0$  is the yield surface location corresponding to the mean normal gravity stresses  $p'_{\text{in}}$ . The initial void ratios are then calculated using  $p'_{\text{in}}$ , the known void ratio at  $p' = 1\text{kN/m}^2$ , and the slope of the normal consolidation line  $\lambda$ . Since collapse occurs at a much larger footing displacement than for the Mohr-Coulomb soil, more increments are needed to apply the displacements. Indeed, for this example, 1,000 increments are used and the ultimate footing displacement is approximately 20 times larger.

The results for the modified Cam clay layer, shown in Table V, include the CPU time for the gravity loading (in parentheses) and the CPU time for the footing loading. Owing to the 20-fold increase in the imposed footing displacement and number of load increments, these analyses consume considerably more CPU time than the runs with the Tresca and Mohr-Coulomb models. Except for the RKDP method, the timings are similar and largely insensitive to the specified error tolerance  $STOL$ . Indeed, the difference in the CPU time for the modified Euler method with  $STOL = 10^{-1}$  and  $STOL = 10^{-4}$  is less than 0.6 percent. The final collapse pressures for the stress integration

Scheme	CPU time (s)	Collapse pressure ( $w/c$ )	Total success. substeps	Max. success. substeps	Stress error ( $\sigma_{\text{error}}$ )
Modified Euler					
$STOL = 10^{-1}$	1,410 (51)	57.823	796,426	5	$0.11 \times 10^{-2}$
$STOL = 10^{-2}$	1,410 (51)	57.733	796,762	10	$0.13 \times 10^{-3}$
$STOL = 10^{-3}$	1,411 (51)	57.718	798,717	19	$0.50 \times 10^{-4}$
$STOL = 10^{-4}$	1,419 (51)	57.718	833,550	37	$0.16 \times 10^{-4}$
Runge-Kutta-Dormand-Prince	2,525 (51)	57.717	3,463,793	185	–

**Table V.**  
Rigid strip footing on associated modified Cam clay layer

Scheme	CPU time (s)	Collapse pressure ( $w/c$ )	Total success. substeps	Max. success. substeps	Stress error ( $\sigma_{\text{error}}$ )
Modified Euler					
$STOL = 10^{-1}$	1,810 (51)	40.911	504,170	21	$0.34 \times 10^{-1}$
$STOL = 10^{-2}$	1,877 (51)	40.507	554,326	57	$0.59 \times 10^{-2}$
$STOL = 10^{-3}$	2,115 (51)	39.898	621,012	129	$0.94 \times 10^{-3}$
$STOL = 10^{-4}$	2,474 (51)	39.260	945,475	278	$0.20 \times 10^{-3}$
Runge-Kutta-Dormand-Prince	4,106 (51)	39.130	4,330,167	878	–

**Table VI.**  
Rigid strip footing on a generalised Cam clay layer

schemes are also close, with a maximum discrepancy of 0.2 percent between the modified Euler run with  $STOL = 10^{-1}$  and the RKDP run (which uses  $STOL = 10^{-9}$ ).

The observed stress errors for the modified Euler scheme again decrease with decreasing values of  $STOL$  and exhibit a “tolerance proportionality”. However, unlike the results obtained for the Tresca and Mohr-Coulomb soils, these errors are about one order smaller than they need to be. This suggests that the explicit approach with automatic substepping is accurate not only for simple elastoplastic models, but also for highly complex models which include non-linear elasticity and hardening.

The footing analyses for generalised Cam clay were conducted in the same way as for modified Cam clay, with the soil layer first being loaded by its own gravity and then by the imposed footing displacements. As shown in Table VI, the generalised Cam clay results give lower limit pressures than those for modified Cam clay. This is consistent with the shapes of the respective yield surfaces in the deviatoric plane, which are shown in Figure 1. Compared to all previous examples, the CPU times for the modified Euler scheme vary more significantly as  $STOL$  is reduced. This sensitivity is also reflected in the collapse pressures, with the modified Euler method differing from the RKDP method by 4.6 percent for  $STOL = 10^{-1}$  and 0.33 percent for  $STOL = 10^{-4}$ . The measured errors in the stresses for the modified Euler method are comparable with the specified tolerances  $STOL$  and exhibit tolerance proportionality. These results indicate the explicit modified Euler method works well for the generalised Cam clay model which has a rounded Mohr-Coulomb yield surface in the deviatoric stress plane.

## 5. Conclusions

The explicit modified Euler method with automatic substepping provides an economical means of integrating a wide range of elastoplastic constitutive laws. Unlike fully implicit methods, the procedure can be implemented in a general way and requires only minor changes to incorporate complex models such as those belonging to the critical state family. Moreover, the substepping mechanism permits the user to control the error in the computed stresses which would otherwise be unknown. This is of particular benefit for highly non-linear problems where, even for small load steps, large strain increments are frequently encountered.

## References

- Abbo, A.J. (1997), “Finite element algorithms for elastoplasticity and consolidation”, PhD thesis, University of Newcastle, Newcastle.
- Borja, R.I. (1991), “Cam-clay plasticity. Part II: implicit integration of constitutive equations based on a non-linear elastic stress predictor”, *Computer Methods in Applied Mechanics and Engineering*, Vol. 88, pp. 225-40.
- Borja, R.I. and Lee, S.R. (1990), “Cam-clay plasticity. Part I: implicit integration of elasto-plastic constitutive relations”, *Computer Methods in Applied Mechanics and Engineering*, Vol. 78, pp. 49-72.

- 
- Britto, A.M. and Gunn, M.J. (1987), *Critical State Soil Mechanics via Finite Elements*, Ellis Horwood, Chichester.
- Conte, S.D. and de Boor, C. (1980), *Elementary Numerical Analysis, An Algorithmic Approach*, 3rd ed., McGraw-Hill, New York, NY.
- Crisfield, M.A. (1991), *Non-linear Finite Element Analysis of Solids and Structures*, Volume 1, John Wiley & Sons, Chichester.
- Crisfield, M.A. (1997), *Non-linear Finite Element Analysis of Solids and Structures*, Volume 2, John Wiley & Sons, Chichester.
- Dowell, M. and Jarratt, P. (1972), "The Pegasus method for computing the root of an equation", *BIT*, Vol. 12, pp. 503-8.
- Lade, P.V. and Duncan, J.M. (1975), "Elasto-plastic stress-strain theory for cohesionless soil", *Journal of Geotechnical Engineering Division, ASCE*, Vol. 101, pp. 1037-53.
- Nayak, G.C. and Zienkiewicz, O.C. (1972), "Elasto-plastic stress analysis: a generalisation for various constitutive relations including strain softening", *International Journal for Numerical Methods in Engineering*, Vol. 5, pp. 113-35.
- Naylor, D.J. (1985), "A continuous plasticity version of the critical state model", *International Journal for Numerical Methods in Engineering*, Vol. 21, pp. 1187-204.
- Ortiz, M. and Simo, J.C. (1986), "An analysis of a new class of integration algorithms for elasto-plastic constitutive relations", *International Journal for Numerical Methods in Engineering*, Vol. 23, pp. 353-66.
- Owen, D.R.J. and Hinton, E. (1980), *Finite Elements in Plasticity: Theory and Practice*, Pineridge Press, Swansea.
- Potts, D.M. and Ganendra, D. (1992), "A comparison of solution strategies for non-linear finite element analysis of geotechnical problems", *Proceedings of the 3rd International Conference on Computational Plasticity*, Barcelona, pp. 803-14.
- Potts, D.M. and Ganendra, D. (1994), "An evaluation of substepping and implicit stress point algorithms", *Computer Methods in Applied Mechanics and Engineering*, Vol. 119, pp. 341-54.
- Potts, D.M. and Gens, A. (1985), "A critical assessment of methods of correcting for drift from the yield surface in elastoplastic finite element analysis", *International Journal for Numerical and Analytical Methods in Geomechanics*, Vol. 9, pp. 149-59.
- Randolph, M.F. (1982), "Generalising the Cam-clay models", Workshop on Implementation of Critical State Soil Mechanics in Finite Element Computation, Cambridge.
- Roscoe, K.H. and Burland, J.B. (1968), "On the generalised stress-strain behaviour of 'wet' clay", *Engineering Plasticity*, Cambridge University Press, Cambridge, pp. 535-609.
- Schofield, A.N. and Wroth, C.P. (1968), *Critical State Soil Mechanics*, McGraw-Hill, London.
- Sheng, D., Sloan, S.W. and Yu, H.S. (1999), "Practical implementation of critical state models in finite element method", *Proceedings of the 8th Australian and New Zealand Conference on Geomechanics*, Hobart, Vol. 2, pp. 975-81.
- Simo, J.C. and Taylor, R.L. (1985), "Consistent tangent operators for rate-independent elasto-plasticity", *Computer Methods in Applied Mechanics and Engineering*, Vol. 48, pp. 101-18.
- Sloan, S.W. (1987), "Substepping schemes for the numerical integration of elastoplastic stress-strain relations", *International Journal for Numerical Methods in Engineering*, Vol. 24, pp. 893-911.
- Sloan, S.W. and Booker, J.R. (1986), "Removal of singularities in Tresca and Mohr-Coulomb yield criteria", *Communications in Applied Numerical Methods*, Vol. 2, pp. 173-9.

- Sloan, S.W. and Booker, J.R. (1992), "Integration of Tresca and Mohr-Coulomb constitutive relations in plane strain elastoplasticity", *International Journal for Numerical Methods in Engineering*, Vol. 33, pp. 163-96.
- Sloan, S.W. and Randolph, M.F. (1982), "Numerical prediction of collapse loads using finite element methods", *International Journal for Numerical and Analytical Methods in Geomechanics*, Vol. 6, pp. 47-76.
- Van Eekelen, H.A.M. (1980), "Isotropic yield surfaces in three dimensions for use in soil mechanics", *International Journal for Numerical and Analytical Methods in Geomechanics*, Vol. 4, pp. 89-101.
- Wissmann, J.W. and Hauck, C. (1983), "Efficient elastic-plastic finite element analysis with higher order stress point algorithms", *Computers and Structures*, Vol. 17, pp. 89-95.
- Yamaguchi, E. (1993), "A comparative study of numerical methods for computing stress increments in elastic-plastic materials", *Proceedings of the Asia-Pacific Symposium on Advances in Plasticity and Its Applications*, Hong Kong, pp. 625-30.